MICROCOPY RESOLUTION TEST CHART

NATIONAL BUREAU OF STANDARDS-1963-A

Contract N00014-83-C-0105
University of California, San Diego

UNIVERSITY OF CALIFORNIA

San Diego

Studies on the Mechanics of Rapidly

Flowing Granular-fluid Materials

A dissertation submitted in partial satisfaction of the

requirements for the degree Doctor of Philosophy

in Oceanography

by

Daniel Martin Hanes

Committee in charge:

    Professor Douglas L. Inman, Chairman

    Professor Joseph R. Curray

    Professor Albert T. Ellis

    Professor Robert T. Guza

    Professor Stanley Middleman

    Dr. Richard J. Seymour

1983

This dissertation of Daniel Martin Hanes is approved,

and is acceptable in quality and form for

publication on microfilm:

Stanley Flagg

Jack R. Cunny

Albert T. Ellis

Richard Seymour

R. T. Guza

Douglas L. Inman   Chairman

University of California, San Diego

1983

iii

Table of Contents

LIST OF SYMBOLS

A	function representing anisotropy of granular collisions
B	Bagnold number $(\rho_s \lambda^{\frac{1}{2}} D \frac{dU}{dz} / \mu)$
$\vec{B}$	body force
D	grain diameter
ΔE	ratio of kinetic energy generated to kinetic energy dissipated in a granular collision
e	internal energy; coefficient of elasticity of a grain
F	a function of N, different in different theories; a force
$\vec{g}$	gravity
K_i	constants
N	volume concentration
N_c	volume concentration at which free energy is a minimum
N_m	maximum volume concentration
N_o	volume concentration at the surface of a flow
P	pressure
Q	heat flux through boundary
$\vec{q}$	heat flux
R	ratio of collisional forces to viscous forces
Re	Reynold's number
s	separation distance between grains
$\overset{=}{T}$	stress tensor
t	time
U	velocity of grains

U_m	the characteristic, or maximum velocity
u	velocity of fluid
x	spacial coordinate, usually direction of flow
y	spacial coordinate, usually in cross-flow direction
Z_o	thickness of motion
z	spacial coordinate, usually vertical
α	function of N in constitutive theories, different for different theories
β	an angle, usually slope of inclined plane
Γ	a constant $= \frac{dN}{dz}$ in McTigue's theory
γ	heat source
Θ	pseudo-temperature (mechanical analogy to temperature)
κ	"mechanical" thermal conductivity
λ	linear concentration, D/s
μ	fluid viscosity
π	3.14159....
ρ	density
ρ_f	fluid density
ρ_s	solid grain density
τ	a stress
τ_o	applied shear stress
τ_n	applied normal stress
$\overset{=}{T}$	"rate of deformation" tensor
ϕ	friction angle
ϕ_i	friction angle for initial yield

ϕ_r or ϕ_d friction angle for residual, or dynamic yield

$\bar{\bar{I}}$ identity tensor

-   superscript indicating vector

=   superscript indicating tensor

Notation

Indicial notation is used when convenient:

Repeated indices indicate summation.

A comma followed by an index indicates

differentiation with respect to the index.

e.g.: $U_{i,i} = \dfrac{dU_1}{dx_1} + \dfrac{dU_2}{dx_2} + \dfrac{dU_3}{dx_3}$

∇ gradient operator

e.g.: $\nabla \cdot \bar{T} = T_{ij,j}$ (i equations)

'   Indicates derivative when function only depends on

one variable (usually z).

e.g.: $U' = \dfrac{dU}{dz}$ if U is a function of z only

$\dfrac{D}{Dt}$ Material derivative $= \dfrac{d}{dt} + U_i \dfrac{d}{dx_i}$

e.g.: $\dfrac{D\bar{U}}{Dt} = \dfrac{d\bar{U}}{dt} + U_1\dfrac{d\bar{U}}{dx_1} + U_2 \dfrac{d\bar{U}}{dx_2} + U_3\dfrac{d\bar{U}}{dx_3}$

List of Figures

List of Tables

Acknowledgements

I wish to acknowledge and thank:

My committee, for their guidance and patience. Professor D.L. Inman, for his support, advise, and for allowing me to learn about his view of the world. Dick Seymour, for nearly a decade of enthusiasm, encouragement, scientific insight, and friendship. Bob Guza, for his keen editorial eye, his critical thinking, and his endurance. Mike Clark, for drafting the figures and for his ribald humor. Mert Ingraham, for machining the shear cell.

The students and staff of the Shore Processes Lab, the Hydraulics Lab, and the Nearshore Research Group, for knowing how to make work pleasurable.

Steve Pawka, for helping me maintain a level perspective when black looked like white, and white like black. Margie Edwards, for her moral support, and for helping prepare this thesis. Rusty Erdman, for helping me maintain a semblance of sanity during the last few months.

Hank Aaron and Sandy Koufax, who first impressed upon me the impact of a collisional interaction.

Everyone who has shared a beach fire or the warmth of friendship with me.

Mom and Dad, without whom I wouldn't be here.

VITA

Born May 26, 1955 - Dallas, Texas

1977   B. A., Applied Mechanics and Engineering Science, University
          of California, San Diego

1979   M. S., Oceanography, Scripps Institution of Oceanography,
          University of California, San Diego

1977 -   Research Assistant, Scripps Institution of Oceanography,
Present   University of California, San Diego

Publications

"Performance analysis of a tethered float breakwater," (with R. J.
Seymour), The Journal of the Waterway Port Coastal and Ocean Division,
v. 105, n. WW3, 1979.

"F eld measurements of bed and suspended load motion in the surf zone,"
(with D. L. Inman), p. 217-218, Proc. 17th Int. Conf. on Coastal
Engineering, abstracts vol., 456 pp., 1980.

"Field measurements of sand motion in the surf zone," (with D. L.
Inman, J. A. Zampol, T. E. White, B. W. Waldorf and K. A Kastens),
Proc. 17th Int. Conf. on Coastal Engineering, Am. Soc. Civil Eng., 1980.

"Rheology of granular-fluid material," p. 49-53 in Fluid-sediment
interactions on beaches and shelves, progress report, 1980-1981,
(D. L. Inman, R. T. Guza, C. D. Winant and R. E. Flick). SIO Reference
Series 81-27, 1981.

"Vertical mixing in surf zone sand beds," Transactions, American
Geophysical Union, v. 63, n. 3, p. 64 (abstract only), 1982.

"Rapid shear flow in a granular bed," presented at the International
Union of Theoretical and Applied Mechanics Symposium on Deformation
and Failure of Granular Materials, Delft, 1982.

FIELDS OF STUDY

Major Field: Oceanography

    Studies in Physical Oceanography
        Professors R.T. Guza, M.C. Hendershott,

        W. Munk, R.L. Salmon, and J.L. Reid

    Studies in Nearshore Processes

        Professor D.L. Inman

    Studies in Marine Chemistry

        Professor J. Gieskes

    Studies in Biological Oceanography

        Professor M.M. Mullin

    Studies in Marine Geology

        Professors G. Arrhenius, W.H. Berger

        J.R. Curray, and J.W. Hawkins.

    Studies in Applied Mathematics

        Professor S. Rand

1. Introduction

Theoretical and experimental studies on the rapid flow of granular materials have increased in number and significance during the past ten years. This is due in part to the relevence of these flows to a variety of problems of industrial and geophysical significance. Landslides and snow avalanches, the bedload transport of coarse grained sediments, and the saltation of sand grains in air (Owen,1964) can all be treated as flowing granular materials. Analogously, the flow of seeds and grains in hoppers, pharmaceutical powders, and slurries of coal in air or water are examples of important granular flows in industrial processing.

The surge in interest is presumably due also to the intriguing nature of rapid granular flows. The study of these flows cuts across traditional disciplinary boundaries, with contributions being made by applied and theoretical mathematicians and mechanicians, chemical engineers, geoscientists, numerical analysts, and others.

Although there has been much progress made in understanding the flow of granular materials, there are still many conflicting theories, few consistent observations, and several unaddressed questions.

1

1.1 Definitions and characteristics of a

granular-fluid material

A granular material can be defined as an assembly of discreet particles confined by either a body force or physical boundaries. The voids between individual grains may be filled with a fluid such as air or water, or by a vacuum as in the ice rings of Saturn. When subjected to the proper forces and boundary conditions the material may deform in a manner similiar to a fluid. Hence this two-component mixture has been called a granular-fluid material (Inman et.al.,1966), although under some conditions the true fluid component may be inconsequential to the granular flow.

A principal property of granular-fluid materials is that the volume concentration is related to the deformation of the material. The volume concentration is defined as the portion of the total volume which is occupied by the granular component. The importance of the volume concentration was first identified by Reynolds(1885). Reynolds observed that a packed granular material must undergo volumetric expansion in order to deform. He referred to this behavior as dilatency. The term dilatency has subsequently been extended to describe those materials in which the rate of deformation and the volume concentration or density are inversely related for a given stress state.

As implied above, a granular material may deform in a variety of ways in response to applied stresses. The nature of this deformation is governed by the granular concentration, N, and by the ratio of the shear stress to the normal stress (Terzhagi,1943), which will be referred to as the stress ratio (Txz/Tzz).

At high concentrations and low stress ratios the material behaves elastically, with all grains initially in contact remaining in contact. As suggested by Coulomb(1773), when the stress ratio reaches the critical, or static yield value, denoted as $\tan\phi_i$ the material begins to undergo a slipping and rolling type of deformation, in which grain layers may override one another for large distances at low shear rates. At higher shear rates and lower volume concentrations, the stresses become dependent upon the rate of deformation. Collisions between grains play a dominant role, and the interstitial fluid may be inconsequential to the dynamics. This corresponds to the grain-inertia regime first described by Bagnold(1941,1954), and this rapid flow regime is the primary area of interest in this work.

1.2 Previous theoretical approaches

There is a large body of literature dealing with the slow deformation of granular materials at relatively high concentrations (e.g. Vermeer, 1982). Since Drucker and

Prager (1952) applied the associated flow rules of plasticity to soil mechanics, there have been many attempts to treat granular materials as plastic media. Non-associated flow rules have also been proposed by de Josselin de Jong (1959,1971), Spencer(1964), and others. The various advantages and shortcomings of these theories are discussed in Mandl and Luque (1970) and Mehrabadi and Cowin (1978). Although several of these theories have value for the quasi-static flows expected in soil mechanics and for the flow of grains in bins and hoppers, they are not applicable to rapid flow conditions where the stresses are expected to depend on the rate of deformation of the material.

In this work the discussion will be restricted to *rapid shear flows* of granular materials in which dilatency and shear rate dependence of the stresses are important. The theories describing rapid granular flows which account for dilatency and rate dependent stresses can be conveniently divided into those which are derived from consideration of particle interactions and those which are deduced from continuum mechanical and thermodynamic considerations.

The continuum approach is exemplified by Goodman and Cowin (1972), McTigue(1979), and Passman et.al.(1980). In these theories the volume concentration is considered as an independent field variable. Forms for the free energy, entropy, etc., are postulated and the constitutive behavior is subsequently deduced from thermodynamic constraints or,

at times, suggested in an ad-hoc manner. A common feature
of theories utilizing this approach is that there are
generally several undetermined parameters, and sometimes
undetermined functions. This makes experimental
verification extremely difficult (see Bailard(1978), for
example). A strong supporting feature of these theories, on
the other hand, is that they either incorporate or predict
a Coulomb yield condition for initial failure.

For the particle interaction approach, the
constitutive behavior of the assembly is formulated by
examining the interactions between individual grains. The
primary mechanism for stress transfer is a granular
collision. Bagnold (1954) considered the mean paths of
particles undergoing simple shear deformation in order to
formulate the stresses resulting from intergranular
collisions. More recently, McTigue(1979), Ogawa(1978;1980),
Savage and Jeffrey (1982), and Jenkins and Savage (1983)
have included the fluctuating component of velocity in
modeling the collisional stress transfer in a manner
analogous to kinetic theory of gases. Ackermann and Shen
(1982) also consider the stresses resulting from particle
and fluid translations.

The particle interaction approach is more satisfying
than the present state of the continuum approach from a
physical point of view. Furthermore, it predicts stresses
which are quadratic in shear rate, in agreement with several
observations.

1.3 Previous experimental work

The experimental observations of rapid granular flows have primarily been concerned with two types of flow: shear flow between concentric cylinders or parallel plates, and gravity flow down inclined chutes and channels. The earliest , and still the most consistent measurements of granular fluid flow between concentric cylinders were made by Bagnold(1954). Savage and McKeown (1983) have subsequently repeated and extended Bagnold's work. Savage and Sayed(1983) have studied similiar flows between parallel plates in an annular shear cell. There have been many attempts to experimentally study gravity flow down inclines, including Savage(1978), Bailard(1978), and Ishida and Shirai (1979). A good review of these flows is presented in Savage (1982). Numerical simulations of rapid granular shear flows have been carried out by Cambell(1982).

For the case of shear flow between moving boundaries, accurate point measurements of velocity and concentration have proven to be quite elusive. Researchers have been consequently forced to accept the standard rheological techniques of measuring stresses and velocities at the boundaries of the flow, and the average concentration within the flow.

Bagnold(1954) studied the flow of neutrally bouyant spheres immersed in fluid and sheared between concentric

cylinders. He demonstrated the existence of a normal
dispersive pressure which was proportional to the shear
stress. The data also strongly supported the concept that
stress transfer is due to collisional interactions between
grains. Both of these observations have been duplicated by
Savage and McKeown(1983). Savage and Sayed(1983)
experimentally studied the rapid flow of granular materials
(in air) in an annular, parallel plate shear cell. Their
results further confirmed the quadratic rate dependence of
the stresses. Savage and Sayed's measurements of the stress
ratio were higher than Bagnold's, and showed some dependency
upon the volume concentration.

The steady flow of granular material down inclined
chutes and channels has prompted considerable discussion,
with several apparently contradictory observations being
published. Most of these contradictions have been explained
by considering the effects of different materials and
boundary conditions. On the basis of Bailard's and Savage's
works, it is safe to conclude that steady flows are indeed
possible over a range of inclinations. Beyond this
conclusion these experiments have added little to the
general understanding of granular flows. They do, however,
illustrate the lack of understanding for those flows in
which the body force (usually gravity) plays an important
role in determining the velocity and concentration structure
within the flow.

This is an important consideration for almost all geophysical flows because the flow thickness is generally limited in some manner by gravity. The question of the thickness of motion is a central question which will be addressed in this work.

1.4 The thickness of motion

One of the least understood parameters determining the bedload transport of granular sediments is the thickness of motion in the bed (Komar and Inman, 1970; Inman and Hanes, 1980). There is an analogous uncertainty with avalanches, debris flow, mud flows, and the slip faces of sand dunes. The thickness of motion in these granular-fluid flows would be predictable if the complete constitutive behavior of the material were known. However, the constitutive behavior is not known over all ranges of the stress ratio and the volume concentration, hence the prediction of a thickness of motion based upon the equations of motion is quite unlikely. This is because the mechanisms for stress tranfer are likely to change as the level of no motion is approached. Collisions between grains probably become less dominant as sliding friction due to rubbing contact increases.

Bagnold's solution to this problem was to impose a yield criterion at the boundary between moving and stationary grains. He suggested a Coulomb yield criterion,

much like the residual angle of sliding friction in soil
mechanics. Bagnold used this fundamental assumption in the
derivation of nearly all of his sediment transport theory
(1956,1966), as did Bailard and Inman(1979) in their
rederivation of Bagnold's results.

Despite the acceptance and use of the assumption of
a dynamic yield criterion for granular shear flows, the
yield criterion had not been experimentally tested for these
flows prior to the present study.

1.5 Guide to this dissertation

In the next section the deformation of a granular
bed subjected to gravity and to traction applied to its
surface is considered. It is demonstrated that as a
consequence of momentum conservation, the stress ratio
(shear stress/normal stress) must decrease with increasing
depth in the bed, resulting in an internal boundary
separating a shearing region (above) from a rigid
region(below). Constitutive theories for rapidly flowing
granular-fluid materials are presented and applied to this
flow. Original analytic solutions corresponding to
McTigue's constitutive theory and numerical solutions
corresponding to Jenkins and Savage's constitutive theory
are presented. An approximate analytic solution to Jenkins
and Savage's theory is also presented, following the
developments of Jenkins and Savage(1983). The analytic and

numerical solutions suggest a finite thickness of motion.
They also demonstrate the dilatant nature of granular-fluid
materials, the effects of the kinetic energy involved in the
velocity fluctuations, and the importance of the boundary
conditions upon the flow.

Section 3 describes the experimental considerations.
Experiments are performed in an annular shear cell of mean
radius 12.4 cm. The granular materials included two sizes
(1.1mm and 1.85mm) of spherical glass beads, and natural
sand(0.55 mm). Both water and air are used as interstitial
fluids. The approximations involved in interpreting the
experimental data are examined. These include the effects
of rotation, measurement accuracies, and unsteadiness in the
flow.

Section 4 presents the results of the experiments
and compares these results to the constitutive theories.
The stresses are found to be quadratically dependent upon
the shear rate, in agreement with the collisional models of
momentum transfer. Stresses are also found to be weakly
dependent upon the volume concentration at low
concentrations, and strongly dependent at higher
concentration. The existence of an internal boundary is
repeatedly observed. The thickness of the shearing region
varies between 5 and 15 grain diameters. The stress ratios
are approximately constant, with a slight dependence on the
shear rate and volume concentration. The total immersed
weight of the grains in the shearing region is caculated by

applying a dynamic Coulomb yield criterion at the internal

boundary. Measurements are in fair agreement with the

predicted values.

2. Theoretical considerations

Several theories for the constitutive behavior of rapidly flowing granular-fluid materials are presented here. These, along with the basic balance laws for mass, momentum, and energy are applied to the steady, rapid, shear flow of a cohesionless granular bed subjected to gravity and surface traction. The results show why there is a level, called the level of no motion, below which grains remain rigidly locked together.

The granular material will sometimes be considered as a continuum, and sometimes as an assembly of particles. Physical descriptors at a point, such as bulk density or velocity, must be considered in the continuum context as properties averaged over the scale of several grains. The velocity will be treated as the sum of a mean translation and a fluctuation about the mean. The spin of individual grains in not explicitly considered. The grains are assumed to be cohesionless, with no chemical or electrostatic interactions.

The effects of an interstitial fluid are neglected in this analysis. This is a valid approximation when the forces resulting from grain-to-grain interactions are much greater than those resulting from fluid-to-grain interactions, and the influence of the fluid upon the grain-to-grain interactions is unimportant. The conditions under

12

which this approximation is valid are discussed in greater
detail in section 3.5.3.

2.1 The balance laws

The balance laws for mass, linear momentum, angular
momentum, and energy can be written as:

$$\frac{D\rho}{Dt} + \rho U_{i,i} = 0 \qquad\qquad 2\text{-}1a$$

$$\rho \frac{DU_i}{Dt} = T_{ij,j} + \rho b_i \qquad\qquad 2\text{-}2$$

$$T_{ij} = T_{ji} \qquad\qquad 2\text{-}3$$

$$\rho \frac{De}{Dt} = T_{ij} T_{ij} - q_{i,i} + \rho\gamma \qquad\qquad 2\text{-}4$$

where:

$$\rho = \rho_s N \quad \text{(bulk density)} \qquad\qquad 2\text{-}5a$$

$$2T_{ij} = U_{i,j} + U_{j,i} \quad \text{("rate of deformation" tensor)} \qquad 2\text{-}5b$$

$\overline{b}$ is a body force

e is the internal energy

$\overline{q}$ is the heat flux

γ is a heat source

The mass conservation equation, 2-1, can be
rewritten for materials with incompressible grains by
substituting the definition of bulk density, giving:

$$\frac{DN}{Dt} + NU_{i,i} = 0 \qquad\qquad 2\text{-}1b$$

The momentum equation, 2-2, is a balance between accelerations, on the left side, and the combined forces represented by the divergence of the stress tensor and a body force, both on the right side. The absence of coupled stresses is evidenced in the conservation of angular momentum, indicating a symmetric stress tensor (equation 2-3).

From the energy equation (2-4) it can be seen that there are three mechanisms by which the internal energy can be altered. The first is via dissipation due to the deformation, the second is a net flux of heat due to heat flux gradients, and the third is some unspecified heat source (or sink).

2.2 Flow in a semi-infinite, granular bed

Consider a bed of cohesionless grains oriented with its surface perpendicular to the gravity field, as shown in Figure 2-1. If traction, $\bar{\tau} = \tau_o + \tau_n$, is applied to the surface of the bed, the granular material will deform. Consider the case of steady shear deformation in which the mean paths of all moving grains are horizontal, and there are no gradients in the direction of mean flow. In this case the mass balance is identically satisfied, and the linear momentum conservation equation reduces to:

$$T_{ij,j} = \rho_s N b_i \qquad\qquad 2\text{-}6a$$
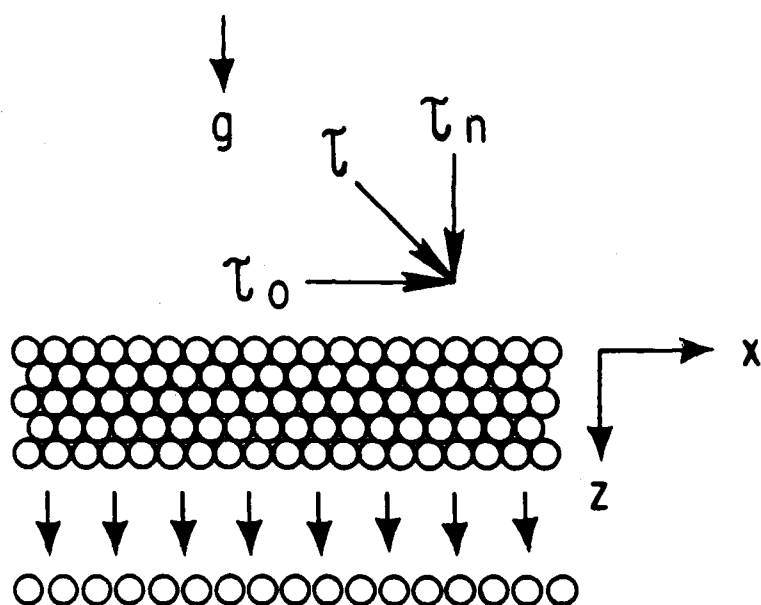
Figure 2-1.   Definitions for a semi-infinite
granular bed subject to surface traction and gravity forces.

Expressing this in terms of the x,z coordinate system depicted in Figure 2-1:

$$T_{xz,z} = 0 \qquad\qquad\qquad 2\text{-}6b$$

$$T_{zz,z} = -\rho_s Ng \qquad\qquad\qquad 2\text{-}6c$$

Integrating these equations and applying the boundary conditions:

$$\left. \begin{array}{l} T_{xz} = \tau_0 \\[2mm] T_{zz} = \tau_n \end{array} \right\} \text{ at } z = 0 \qquad \begin{array}{l} 2\text{-}7a \\[2mm] 2\text{-}7b \end{array}$$

gives:

$$T_{xz} = \tau_0 \qquad\qquad\qquad 2\text{-}8a$$

$$T_{zz}(z) = \tau_n + \int_o^z \rho_s Ng \, dz \qquad\qquad 2\text{-}8b$$

The shear stress remains constant at all depths, equal to the applied shear stress. If the shear stress were to change with depth, the deformation would be unsteady. The normal stress is an increasing function of depth. This is due to the weight of the grains. The ratio of the shear stress to the normal stress decreases with increasing depth in the bed, and eventually the flow presumable must cease. As the depth increases, the situation is analogous to piling more logs on a horse-drawn sled. Eventually the load becomes too heavy for the horse to pull.

Following the well established Coulomb yield criterion for static yield, it is useful to define a Coulomb yield criterion for dynamic yield, corresponding to the limiting value of the stress ratio at which motion ceases. If this concept is valid, then at the boundary between

mobile and immobile grains, the stress ratio should be constant for a given material. The stress ratio can be expressed as a dynamic friction angle:

$$\text{shear stress/normal stress} = \tan\phi_r \qquad 2\text{-}9$$

A simple physical argument supporting the concept that the stability of a stationary grain is determined by the ratio of the shear and normal forces exerted on the grain is shown in Figure 2-2. Grain A is subjected to a normal stress, F_n, and a shear stress, F_o. If the applied stresses combine to result in a net torque about the point of contact, c, the grain will begin to roll. In terms of the stresses and the angle β , this condition is simply:

$$\frac{F_o}{F_n} \geq \tan(\beta) \qquad 2\text{-}10$$

The angle β , and analogously, the angle of dynamic friction, ϕ_r , are expected to be functions of the packing and material characteristics.

This approach is somewhat simplistic since one must consider the mechanics of the actual forces which act on an individual grain and not simply the continuum quantity of stress. In fact, the forces acting on a grain depend upon the nature of the packing, the deformation, and the properties of the granular-fluid material. The forces which one grain can exert on a second grain can be transmitted in three ways: grains may collide and impart momentum to one another, they may push against each other in response to a
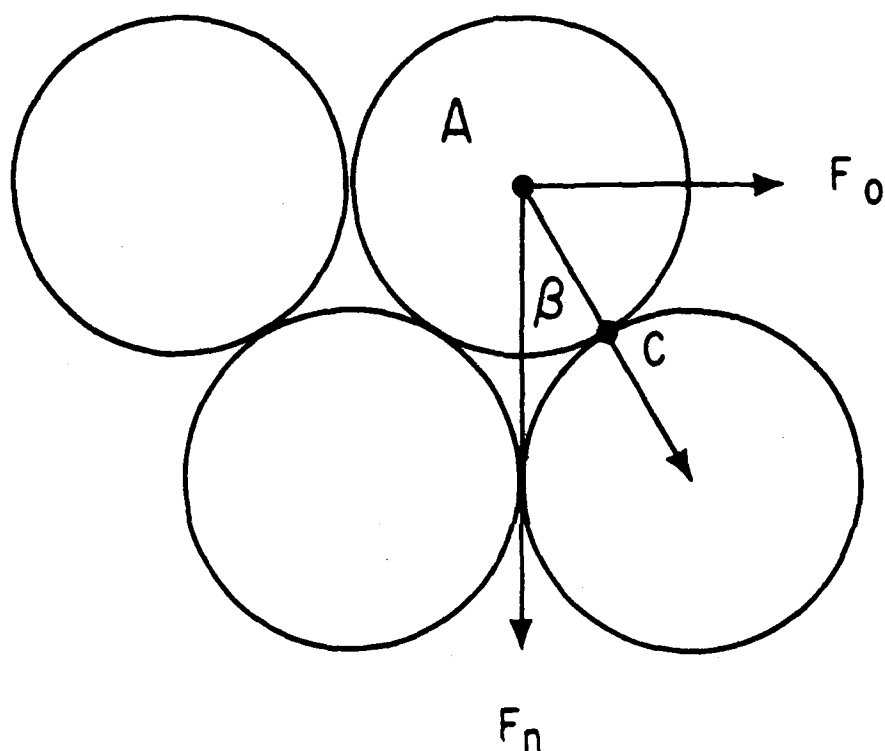
Figure 2-2. Stability diagram for grain A. Grain A will begin to roll about point C if:

$$\frac{F_o}{F_n} \geq \tan\beta$$

body force or an applied stress, or they may frictionally
stress each other by sliding over one another while
resisting relative motion. The second two processes usually
occur together and require approximately continuous contact.

If material at rest is packed in a rigid or near
rigid state, as it is prior to static yield, then the
frictional forces acting on a grain are probably well
represented by the average stress state. The resistance to
relative motion arises from static friction, and the well
established Coulomb yield criterion thus is consistent on a
macroscopic scale. After, but still near the initial yield
point, the frictional forces are still well represented by
the average stress state, and resistance to relative motion
arises from sliding friction. This resistance is generally
less than that of static friction, so the coefficient of
friction is lower. Thus the residual angle of internal
friction in soil mechanics is less than the static angle as
discussed by Bagnold (1966).

In flows where the moving grains are no longer
tightly packed, contact between grains is intermittant
because of collisional interactions. The forces acting on a
grain can momentarily be greater or less than those
described by the average stress state. The stress ratio
could vary considerably, depending on the concentration and
shear rate.

It is interesting to note that a knowledge of $\tan\phi_r$
allows for the prediction of the total immersed weight of

the moving grains. Combining equations 2-8 and 2-9 and
modifying the density to allow for possible buoyancy effects
of the immersing fluid gives:

$$\int_0^{Z_0} (\rho_s - \rho_f) \, Ng \, dz = \frac{\tau_0}{\tan(\phi_r)} - \tau_n \qquad \qquad 2\text{-}11$$

where Z_0 is the depth in the bed at which motion ceases.

In the case where the applied stress is purely shear
and the normal force is due solely to the immersed weight of
the grains, equation 2-11 is a very simple relation relating
these two quantities. As mentioned previously, this
relation is a fundamental assumption underlying much of
Bagnold's work on sediment transport.

2.3 Constitutive models for rapidly flowing,
    granular-fluid materials

The first model to be presented was formulated by
R.A. Bagnold (1954), when he published the results of a
remarkable set of experiments investigating the simple shear
flow of a granular-fluid suspension. Bagnold demonstrated
the importance of granular collisions, particularly for
rapid flows. In the second model presented, McTigue(1979)
modifies Bagnold's theory by adding a frictional stress
which is expected to be important for flows near the initial
yield point. In the third formulation discussed, Savage and
Jeffrey(1981), and Jenkins and Savage(1983) approach the

collisional problem in a manner analogous to the kinetic
theory of gases. Their results are shown to be consistent
with Bagnold's for the simple shear flow of neutrally
buoyant spheres.

2.3.1   The grain-inertia regime of Bagnold

Bagnold(1941,1954) was first to discover and explain
the non-Newtonian nature of rapid granular-fluid shear flows
when he recognized the importance of granular collisions.
By considering the mean paths of grains undergoing rapid,
shear deformation, Bagnold recognized that both the momentum
transferred per collision and the frequency of granular
collisions are proportional to the mean shear rate (see
Figure 2-3), resulting in tangential and normal stresses
quadratic in the mean shear rate. Bagnold experimentally
verified this quadratic dependence of the stresses, as well
as the dependence of the stresses upon the volume
concentration, by studying the flow of neutrally buoyant
spheres sheared between concentric cylinders, as shown in
Figure 2-4. The apparatus was cleverly constructed to allow
for measurements of the shear stress and also of the normal
stress as a function of the mean granular concentration and
the mean shear rate. Combining theory with observations,
Bagnold proposed the following constitutive relations for
the grain-inertia regime:
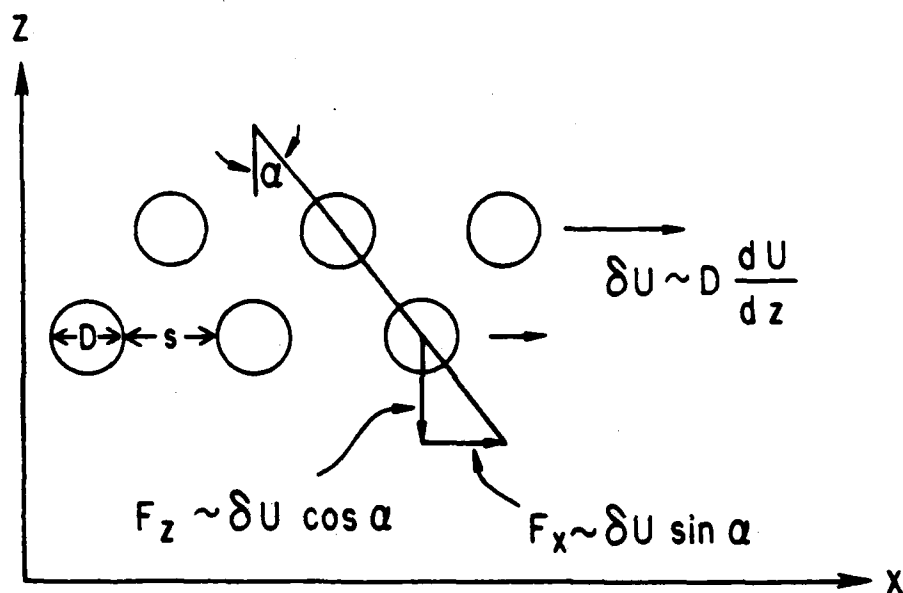
Figure 2-3. Definitions for Bagnold's formulation. F_x and F_z are the forces that result from a collision between two grains moving at relative velocity δU.

RIGID ROTATING
CYLINDER

STATIONARY
DEFORMABLE WALL OF
SHEET RUBBER

T_{zz} T_{xz}

DISPERSED
GRANULAR SOLIDS
IN FLUID
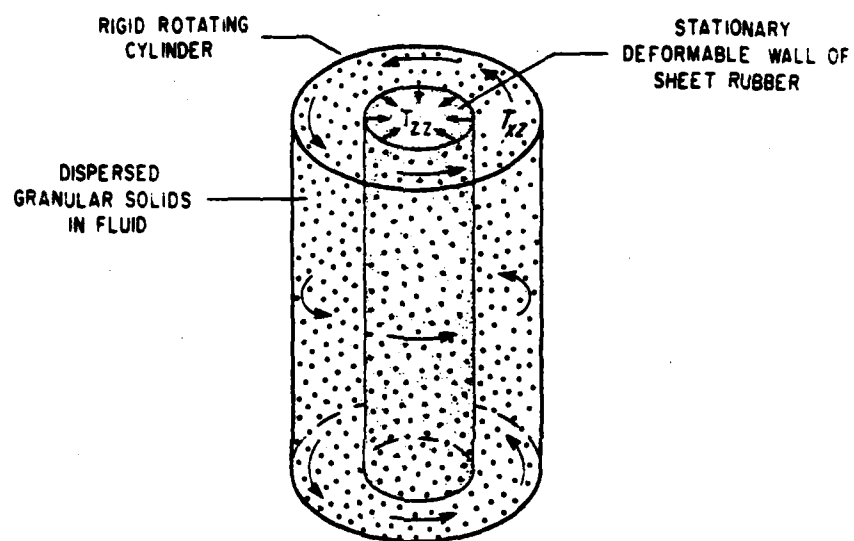
Figure 2-4.   Schematic of Bagnold's apparatus.

$$T_{xz} = .013 \, \rho_s \, (\lambda D U')^2 \qquad\qquad \text{2-12a}$$

$$T_{zz} = .041 \, \rho_s \, (\lambda D U')^2 \qquad\qquad \text{2-12b}$$

where U' ($= \frac{dU}{dz}$) is the mean shear rate and

where λ, the linear concentration, is the ratio of the grain diameter to the mean free separation distance between grains (D/s in Figure 2-3). λ is given as a function of the volume concentration by:

$$\lambda = [(\frac{N_m}{N})^{\frac{1}{3}} - 1]^{-1} \qquad\qquad \text{2-13}$$

where N_m is the maximum possible concentration.

These relations were experimentally verified for

$$B \geq 450 \text{ and } .14 \leq N \leq .60 \ (1.4 \leq \lambda \leq 14) \qquad\qquad \text{2-14}$$

where :

$$B = \frac{\lambda^{\frac{1}{2}} \, \rho_s D^2 U'}{\mu} \qquad\qquad \text{2-15}$$

is the Bagnold number, and is analogous to a Reynolds number. The stress ratio, T_{xz}/T_{zz} or $\tan(\phi_r)$ is equal to about 0.32, or $\tan(18°)$. Bagnold suggested that this ratio is constant in the grain-inertia regime. At lower values of B, the stress ratio increased, reaching a maximum value of 0.75 in the macro-viscous regime.

Bagnold's results have stood for nearly 30 years for the conditions under which they were formulated: steady, uniform, simple shear flow of neutrally buoyant granular

materials. In several situations involving more complex
flows or boundary conditions, the application of Bagnold's
relations leads to unrealistic constraints. Complications
arise from one of two sources. First, the stress ratio was
found to be constant in Bagnold's grain-inertia regime
(using neutrally buoyant particles), conflicting with later
observations of flows (of non-neutrally buoyant particles)
in which the stress ratio varies. Second, and more
importantly, the stresses vanish for vanishing mean velocity
gradient because in Bagnold's apparatus there was no source
for granular velocity fluctuations other than the mean
shear.

To demonstrate these limitations we consider three
flows: gravity driven flow down an inclined channel,
gravity driven flow down a vertical chute, and the simple
shear flow described in the previous section.

As presented in Bailard and Inman(1979), for gravity
driven flow down an inclined plane (see Figure 2-5) the
momentum equation for steady flow is simply :

$$\nabla \cdot \bar{T} = -\rho_s \bar{g} N \qquad \qquad 2\text{-}16a$$

or in terms of the coordinates of Figure 2-5 :

$$T_{xz,z} = -\rho_s g N \sin(\beta) \qquad \qquad 2\text{-}16b$$

$$T_{zz,z} = -\rho_s g N \cos(\beta) \qquad \qquad 2\text{-}16c$$

Integrating these equations and applying a stress free
boundary condition at the upper surface yields:
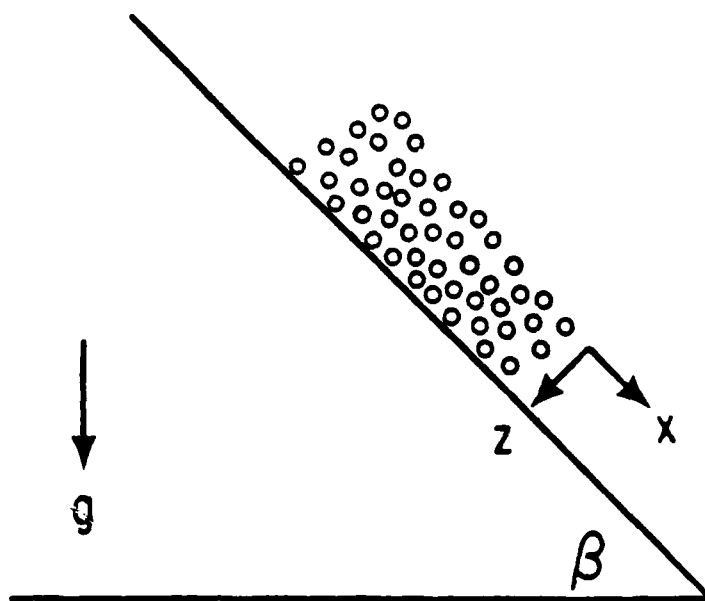
Figure 2-5.   Definitions for inclined plane flow.

$$T_{xz} = -\rho_s g \sin(\beta) \int_0^z N \, dz' \qquad\qquad 2\text{-}17a$$

$$T_{zz} = -\rho_s g \cos(\beta) \int_0^z N \, dz' \qquad\qquad 2\text{-}17b$$

$$\text{and } \frac{T_{xz}}{T_{zz}} = \tan(\beta) \qquad\qquad 2\text{-}17c$$

The stress ratio is constant throughout the flow, and equal to $\tan\beta$ for any slope β. This is in accordance with Bagnold's relations if and only if $\beta = 18°$. In contrast, steady flows of this nature have been reported by Bailard(1978), Savage(1980,1982), and Ishida and Shirai(1982) over a range of inclinations.

A similiar problem arises in the horizontal flow of a granular bed due to traction applied to its upper surface, as discussed previously. It was shown that as a direct result of the conservation of momentum, the stress ratio varied with depth in the flow. Once again, this is inconsistent with Bagnold's observation of a constant stress ratio in the grain-inertia regime.

A third flow, which illustrates the most important shortcoming of Bagnold's relations, is the steady, gravity driven flow down a vertical chute as seen in Figure 2-6. The momentum equation is again

$$\nabla \cdot \bar{T} = -\rho_s N \bar{g} \qquad\qquad 2\text{-}18a$$

Because $\frac{d}{dz} = 0$ for uniform flow, the stresses, velocity, and concentration are fuctions of x only, and equation 2-18a becomes:
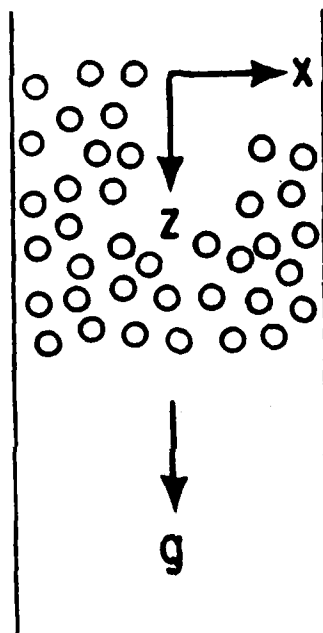
Figure 2-6.   Definitions for vertical chute flow.

$$T_{zx,x} = -\rho_s Ng \qquad\qquad 2\text{-}18b$$

$$T_{xx,x} = 0 \qquad\qquad 2\text{-}18c$$

Because the geometry and forces are completely symmetric about the centerline, symmetry forces U' to vanish at the centerline. But, according to equations 2-12 and 2-18c, if U' vanishes anywhere, it vanishes everywhere, and the flow is inconsistent with equations 2-12 and 2-18.

These obvious limits to Bagnold's relations arise primarily because Bagnold considered the mean paths of the grains, but did not directly consider the fluctuating component of velocity. He was clearly aware of the fluctuating component, as he assumed grain oscillations about the mean path resulted in granular collisions. In fact, if one considers the fluctuating velocity to be driven by the mean velocity gradient, then Bagnold's theory does implicitly consider the fluctuations in a qualitative way. However, by not explicitly treating the velocity fluctuations, there is no clear way to account for the diffusion of fluctuation velocity or the generation of fluctuation velocity by mechanisms other than the mean shear.

The fact that Bagnold's model agrees well with his experiments should not be overlooked. A more sophisticated theory must agree with Bagnold's results for the simple shear flow of neutrally buoyant grains.

2.3.2 McTigue's modification

McTigue(1979,1982) placed the collisional arguments of Bagnold in a more rigorous framework by formulating the stresses resulting from granular collisions as an integral, over all possible collisions, of the momentum transferred in any single two particle (binary) collision. He further suggested that the model could be improved by adding an equilibrium stress to represent the quasi-static stresses which occur when the material is near the initial failure state.

The inclusion of an equilibrium stress is reminiscent of the work of Goodman and Cowin(1970,1971) and Savage(1979). McTigue divides the total stress $\bar{\bar{T}}$, into $\bar{\bar{T}}^{\circ}$, the equilibrium stress, and $\bar{\bar{T}}^{*}$, the dissipative stress due to granular collisions. The form for each of these components of the stress tensor is given below for a cohesionless granular material composed of incompressible spheres:

$$\bar{\bar{T}}^{*} = K_1 (N_m-N)^{-2} \Pi'^{\frac{1}{2}} \bar{\bar{T}} - K_2 (N_m-N)^{-2} \bar{\bar{T}}^2 \qquad \text{2-19a}$$

$$\bar{\bar{T}}^0 = -\alpha (N^2-N_c^2)\bar{\bar{I}} + \alpha\sin\phi(N^2-N_c^2) \Pi'^{-\frac{1}{2}}\bar{\bar{T}} \qquad \text{2-19b}$$

$$\text{where } \Pi' = \frac{1}{2}I - \Pi = \frac{1}{2} \text{ trace } (\bar{\bar{T}}^2) \qquad \text{2-19c}$$

$$I = \text{trace } (\bar{\bar{T}}) \qquad \text{2-19d}$$

$$\Pi = \frac{1}{2} ((\text{trace } \bar{\bar{T}})^2 - \text{trace } (\bar{\bar{T}}^2)) \qquad \text{2-19e}$$

K_1, K_2, and α are non-negative constants of the flow, N_c is the critical value of N at which the free energy of the

material is a minimum (see Goodman and Cowin, 1971, 1972, and Passman, et al., 1980), and ϕ is the internal angle of static friction. The function $(N_m - N)^{-2}$ is an empirical fit to Bagnold's(1954) data, where N_m represents a maximum possible concentration. The dissipative part of the stress tensor is quadratic in the shear rate in accordance with Bagnold's model.

In the limit $\dot{\gamma} \to 0$ the equilibrium stress describes an isotropic pressure $p(N) = \alpha(N^2 - N_c^2)$ and stress components $T_{xz} = -p$, and $T_{zz} = -p \sin\phi$. These components satisfy a Coulomb yield criterion on the plane inclined ϕ as seen in Figure 2-7. On the plane ϕ :

$$\tau_o = p \sin(\phi) \cos(\phi) \qquad\qquad \text{2-20a}$$

$$\tau_n = -p(1 - \sin^2(\phi)) = -p\cos^2(\phi) \qquad\qquad \text{2-20b}$$

$$\left| \frac{\tau_o}{\tau_n} \right| = \tan(\phi) \qquad\qquad \text{2-20c}$$

For simple shear flow the total stress components are:

$$T_{xz} = -\alpha\sin(\phi)(N^2 - N_c^2) - K_1(N_m - N)^{-2}(U')^2 \qquad \text{2-21a}$$

$$T_{zz} = -\alpha(N^2 - N_c^2) - K_2(N_m - N)^{-2}(U')^2 \qquad\qquad \text{2-21b}$$

Although there is little physical justification for the form of the equilibrium pressure term, the theory does have several desirable features. The addition of an equilibrium stress alleviates two of the shortcomings of
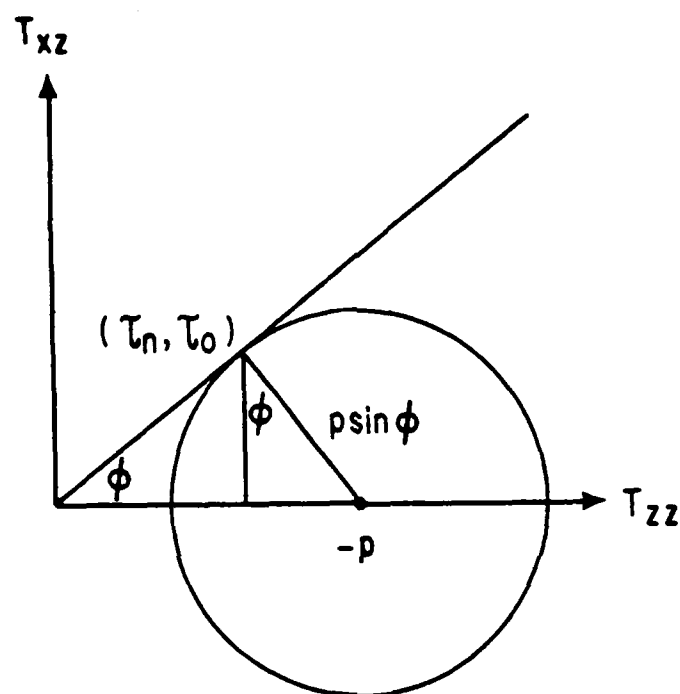
Figure 2-7. Mohr's circle illustrating failure.

plane. On the plane $=\phi$, $\tau_0 = \tau_n \tan(\phi)$.

Bagnold's original constitutive relations by allowing for a
varying stress ratio, and non-zero stresses in the limit of
vanishing deformation. Furthermore, in the limit of
vanishing deformation, the equilibrium stress is in
agreement with a Coulomb criterion for static yield, which
is in accordance with many observations of the behavior of
real granular materials.

One of the major drawbacks of this theory is that it
is nearly impossible to test experimentally because of the
large number of unknown constants and parameters. For
example, the theory is incomplete in its determination of α.
Clearly α is related to the pressure, and its variation
between flows is probably related to the energy tied up in
the random fluctuations in velocity. But since α is not
determined within the theory, it is just another unknown
constant which must be fit to the data.

2.3.3 The "kinetic" theory of Savage, Jeffrey, and Jenkins

Savage and Jeffrey(1981) and Jenkins and
Savage(1983) derive constitutive relations for the rapid
shear flow of cohesionless spheres by explicitly considering
the fluctuating component of velocity in calculating the
momentum transfer due to binary granular collisions.
Following the examples of Ogawa(1978,1980), they consider
the fluctuating component of the velocity to be a
mechanical, or "macroscopic" temperature, which will be

referred to as the pseudo-temperature. The development is analogous to the kinetic theory of gases, with the primary differences being that in a granular-fluid the collisions are driven by the inhomogeneity in the mean flow, and energy is lost via internal dissipation during imperfectly elastic granular collisions.

One of the essential ingredients in the development of these theories was the recognition that the distribution of collisions is anisotropic in a shear flow even though the distribution of grains may be homogeneous. The simple explanation for this is that grains being pushed together by the mean flow are more likely to collide than grains which are being separated from each other by the mean flow.

Savage, Jenkins, and Jeffrey's basic approach is to define the stresses and energy dissipation in terms of integrals over all probable collisions. By assuming a single particle velocity distribution function, and a complete pair distribution function for two particles at contact, these integrations can be carried out.

Savage and Jeffrey assume the single particle velocity distribution function to be Maxwellian about the mean velocity. They derive a complete pair distibution function to be a function of:

$R = D \dfrac{dU}{dz} \overline{(v^2)}^{-\frac{1}{2}}$ = the mean shear characteristic velocity divided by the rms precollisional velocity perturbation.

They can then numerically integrate the collision integrals

for arbitrary R. Unfortunately, R is not determined, but must be guessed or measured for a given flow of any granular material.

Jenkins and Savage modified the theory by assuming the collision distribution function, A, to be linear in the velocity gradient. They suggest using the form:

$$A = 1 - \frac{\alpha \overline{K} \cdot \overline{U}_{12}}{\sqrt{\pi \Theta}}$$

2-22

where $\overline{U}_{12}$ is the relative velocity of colliding grains, $\overline{K}$ is the vector connecting the center of the two grains at collision, and $\alpha(N)$ is an unknown function. This is a simple form which captures the ideas about collision anisotropy expressed above. After carrying out the necessary integrations the following expressions are obtained by Jenkins and Savage:

$$\overline{T} = \frac{\sqrt{\pi \Theta} \, \kappa}{D} \, \overline{I} - \frac{\kappa(2+\alpha)}{5} \, (tr(\overline{\overline{T}})\overline{\overline{I}} + 2\overline{\overline{T}})$$

2-23

$$\overline{q} = - \kappa \nabla \Theta$$

2-24

$$\gamma = \frac{\kappa(1-e)}{2D^2} \left(12\Theta - (3\pi + 4\alpha)D \frac{\sqrt{\Theta}}{\sqrt{\pi}} \, tr(\overline{\overline{T}})\right)$$

2-25

where $\kappa = 2\rho_s N \, g_0(N)\Gamma(1+e) \frac{\sqrt{\Theta}}{\sqrt{\pi}}$,

2-26

$$g_0(N) = \frac{1}{1-N} + \frac{3N}{2(1-N)^2} + \frac{N^2}{2(1-N)^3} = \frac{N(2-N)}{(1-N)^3} ,$$

2-27

e is the coefficient of elasticity of the granular material, and Θ is the pseudo-temperature.

The relative importance of the interstitial fluid
can be estimated in the context of this theory as the ratio
between the "effective" granular viscosity (the ratio of the
shear stress to the shear rate) to the interstitial fluid
viscosity.

$$R = \frac{\rho_s(1+e)(2+\alpha)DN^2\sqrt{\Theta}}{5\mu(1-N)^3\sqrt{\pi}}$$
<div align="right">2-28</div>

This ratio, given by equation 2-28, is analogous to the
Bagnold number in the sense that it represents the relative
importance of grain-to-grain forces compared to fluid-to-
grain forces.

The set of equations 2-23 to 2-27 is closed by
formulating a conservation equation for mechanical energy.
For simple shear flow the energy balance is:

$$(\kappa\Theta')' + T_{xz}U' - \frac{6(1-e)\kappa\Theta}{D^2} = 0$$
<div align="right">2-29</div>

and the stresses are:

$$T_{xz} = \frac{-\kappa(2+\alpha)}{5}U'$$
<div align="right">2-30a</div>

$$T_{zz} = \frac{\kappa\sqrt{\pi\Theta}}{D}$$
<div align="right">2-30b</div>

and $\quad \dfrac{T_{xz}}{T_{zz}} = \dfrac{(2+\alpha)U'}{5D\sqrt{\pi\Theta}}$
<div align="right">2-30c</div>

In equation 2-29, the first term represents the
diffusion of mechanical heat, the second term is the
generation of mechanical heat by the mean shear, and the
last term is the dissipation into actual heat due to
imperfectly elastic granular collisions. Somewhat analogous

to the generation of turbulence in a fluid, there is a cascade of energy from the mean shear into fluctuating kinetic energy, and finally into true heat, as suggested by McTigue(1979) and Jenkins and Cowin(1979).

This theory is physically sound, and experimentally testable since there are relatively few empirical constants. The only unknown quantity which can be experimentally determined is the function $\alpha(N)$. This is simple, particularly for the case in which it is assumed constant. Jenkins and Savage's treatment of the granular collisions is idealistic in the sense that rotation of the grains, frictional forces, and multiple collisions are all ignored. The collision anisotropy is also parameterized in a simple manner. Nevertheless, the approach is rational, physically reasonable, and amenable to inclusion of more complicated granular interactions.

2.4   Application of constitutive theories to shear flow

The constitutive relations of McTigue and those of Jenkins and Savage will now be applied to the flow of a granular bed subjected to gravity and traction to its surface, as discussed previously in section 2.1.

An analytic solution using McTigue's constitutive theory is derived. The solutions closely resemble McTigue's solutions for inclined plane flow. The solutions predict a finite thickness of motion, with the concentration

increasing linearly with depth from a minimum (N_o) at the surface to a maximum (N_b) at the bottom of the moving layer. The velocity is shown to decrease from its maximum (U_m) at the surface to zero at the bottom.

An analytic solution presented by Jenkins and Savage (using their constitutive theory) is given because it represents the solution of the granular bed flow in the limit of vanishing gravity. This solution is testable using a parallel plate shear apparatus, as will be discussed in sections 3 and 4. The exact equations of motion using Jenkins and Savage's constitutive theory are solved numerically. The solutions demonstrate the importance of the boundary condition for the pseudo-temperature. It is also shown that there is a depth in the bed at which the pseudo-temperature reaches a minimum, corresponding to a thickness of "thermalization".

2.4.1 Solutions using McTigue's constitutive relations

Combining McTigue's constitutive relations, equation 2-21, with the momentum conservation equations, 2-6, the following equations of motion are obtained:

$$T'_{xz} = 0 = 2\alpha NN'\sin(\phi) + K_1[(N_m-N)^{-2}(U')^2]' \qquad \text{2-31a}$$

$$-T'_{zz} = \rho_s Ng = 2\alpha NN' + K_2[(N_m-N)^{-2}(U')^2]' \qquad \text{2-31b}$$

Combining these equations in order to obtain an independent

equation for the volume concentration yields

$$N' = \frac{\rho_s g}{2\alpha(1 - \frac{K_2}{K_1} \sin(\phi))} \equiv \Gamma \qquad 2\text{-}32$$

The gradient of N is constant, so the volume
concentration is a linear function of depth in the bed.
Applying the boundary condition

$$N = N_0 \text{ at } z=0 \qquad\qquad 2\text{-}33$$

gives

$$N = N_0 + \Gamma z \qquad\qquad 2\text{-}34$$

The volume concentration increases linearly from N at the
surface.

The velocity gradient, U', can be solved for by
combining equations 2-31 with 2-34 and integrating:

$$-U' = (\frac{\alpha \sin(\phi)}{K_1})^{\frac{1}{2}} (N_m - N) (\frac{\tau_0}{\alpha \sin(\phi)} + N_c^2 - N_0^2 - 2\Gamma N_0 z - \Gamma^2 z^2)^{\frac{1}{2}} \qquad 2\text{-}35$$

The magnitude of the velocity gradient is a maximum
at the surface and decreases with depth, as the
concentration increases. The equilibrium stress increases
with depth as the dynamic, or dissipative stress, decreases.
At some depth the dynamic stresses vanish due to a vanishing
velocity gradient. Noting that

$$2\Gamma N_0 z + \Gamma^2 z^2 = N^2 - N_0^2 \qquad\qquad 2\text{-}36$$

and combining equations 2-35 and 2-36 (for $N < N_m$) reveals:

$$U' \longrightarrow 0 \text{ as } N^2 \longrightarrow \frac{\tau_\theta}{\alpha \sin(\phi)} + N_c^2 \qquad \text{2-37}$$

Thus there is a level of vanishing dynamic stress, denoted by z_0, at which

$$N_b \equiv N|_{z=Z_0} = \left(\frac{\tau_\theta}{\alpha \sin(\phi)} + N_c^2 \right)^{\frac{1}{2}} \qquad \text{2-38}$$

To obtain the velocity profile, equation 2-35 can be directly integrated with the application of the boundary conditions:

$$U = U_m \text{ at } z = 0 \qquad \text{2-39a}$$

$$U = 0 \text{ at } z = Z_0 \qquad \text{2-39b}$$

to give:

$$\frac{U}{U_m} = \frac{N_m N_b^2 \left(\frac{\pi}{2} - \sin^{-1}(\frac{N}{N_b}) \right) - \frac{2}{3}F^{\frac{3}{2}} - N_m N F^{\frac{1}{2}}}{N_m N_b^2 \left(\frac{\pi}{2} - \sin^{-1}(\frac{N_0}{N_b}) \right) - \frac{2}{3}[F(0)]^{\frac{3}{2}} - N_m N_0 [F(0)]^{\frac{1}{2}}}$$

where:

$$F = N_b^2 - N^2 \qquad \text{2-41}$$

$$N = N_0 + \Gamma z \qquad \text{2-42}$$

U/U_m, $(N - N_0)/(N_b - N_0)$, $T_{xz}^*/(T_{xz}^\circ + T_{xz}^*)$, and $T_{xz}^\circ/(T_{xz}^\circ + T_{xz}^*)$ are plotted against nondimensional depth, z/Z_0, for various values of N_0 and N_b in Figure 2-8. It should be noted that neither N_0 nor N_c are known a priori.

As the concentration becomes greater with depth, the velocity gradient decreases, maintaining a constant shear stress. The dissipative stress is a maximum at the surface
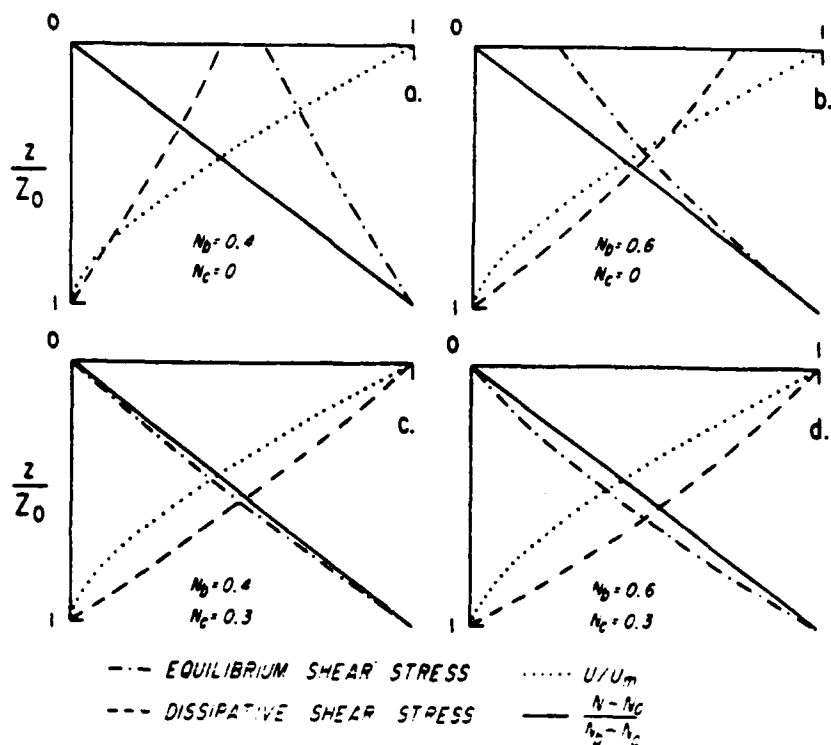
Figure 2-P. Solutions for velocity, volume concentration, and the dissipative and equilibrium components of the stress, based upon McTigue's constitutive theory. The velocity is normalized by its maximum value, the stresses are normalized by the total stress, and the depth is normalized by the thickness of motion, Z_0.

and approaches zero at z_o, the level of no motion. The
equilibrium stress varies in the opposite sense, and the
total shear stress remains constant.

This solution, indicating that the concentration
increases linearly with depth in the flow, is similiar to
the solutions for inclined plane flow presented by
Mctigue(1979). It should be noted, however, that the neither
the measurements of Bailard(1978) nor those of Savage(1978)
support this theory. Rather, these observations suggest that
the concentration is a minimum at the top and bottom of the
flow, and a maximum near the middle of the flow.

At the level of no motion the stresses are

$$T_{xz} = - \alpha(N_b^2 - N_c^2) \sin(\phi) \qquad \text{2-43a}$$

$$T_{zz} = -\alpha(N_b^2 - N_c^2) \qquad \text{2-43b}$$

$$\text{and } \frac{T_{xz}}{T_{zz}} = \sin(\phi) \qquad \text{2-43c}$$

As suggested by McTigue(1979) when he analyzed inclined
plane flow, one could define a dynamic friction coefficient,
$\tan\phi_d$, such that

$$\sin(\phi) = \tan(\phi_d) \qquad \text{2-44}$$

as suggested by equation 2-43c. This is in agreement with
the suggestion earlier of a dynamic Coulomb yield criterion.

2.4.2 Solutions using the 'kinetic' theory
of Jenkins and Savage

Nondimensionalizing terms by D, ρ_s, and g, the momentum equations 2-30 become

$$\frac{(2 + \alpha)\,\kappa U'}{5} = -\tau_0 \qquad\qquad \text{2-45a}$$

$$\sqrt{\pi}(\kappa\sqrt{\Theta})' = N \qquad\qquad \text{2-45b}$$

$$\text{where } \kappa = \frac{N^2(2-N)(1+e)}{(1-N)^3}\frac{1}{\sqrt{\pi}}\sqrt{\Theta} \qquad\qquad \text{2-45c}$$

The energy equation, 2-29, becomes

$$(\kappa\Theta')' - \tau_0 U' - 6(1 - e)\,\kappa\Theta = 0 \qquad\qquad \text{2-46}$$

Equations 2-45 and 2-46 are four equations with four unknown functions of depth, z. These equations are subject to the following boundary conditions at z=0 :

$$U = U_m \qquad\qquad \text{2-47a}$$

$$N = N_0 \qquad\qquad \text{2-47b}$$

$$\sqrt{\pi}\,\kappa\,\sqrt{\Theta} = \tau_n \qquad\qquad \text{2-47c}$$

$$\Theta' = 0 \qquad\qquad \text{2-47d}$$

Boundary conditions a and b are the velocity and concentration at the upper surface of the bed. Boundary condition c indicates the balance between the applied normal stress and the normal stress generated by the deformation of the material. Boundary condition d states that there is no diffusive flux of mechanical temperature at z=0. There is some uncertainty associated with this boundary condition, as discussed by Jenkins and Savage(1983). Since the applied

stresses must result from the interaction of the granular-
fluid material with a boundary, the nature of this
interaction should strongly effect the flux of mechanical
temperature at the boundary.

Possibly a more appropriate boundary condition is:

$$\Theta' = U(U')^2 \qquad\qquad 2\text{-}47e$$

Equation 2-47e is essentially a dimensional argument that Θ
and U' should be of the same order.

2.4.2.1 Analytic solutions using 'kinetic' theory

The set of equations 2-45 to 2-47 can be solved
numerically using standard integration techniques. These
solutions will be presented below, but first analytic
solutions will presented for the limiting case in which the
applied normal stress is much greater than the self weight
of the granular-fluid material undergoing shearing. This is
equivalent to ignoring gravity, thus reducing the problem to
be identical to Bagnold's formulation and experiments. The
development follows Jenkins and Savage(1983).

The boundary condition 2-47c applied to the integral
of equation 2-45b indicates the normal stress is everywhere
equal to the applied normal stress as indicated below:

$$\sqrt{\pi}\, \kappa\, \sqrt{\Theta} = \tau_n \qquad\qquad 2\text{-}48$$

The energy equation 2-46 is transformed by
substituting κ from equation 2-48 and combining equation 2-

45a :

$$\left(\frac{\tau_n}{\sqrt{\pi}} \frac{\Theta'}{\sqrt{\Theta}}\right) + \frac{5\sqrt{\pi}\tau_0^2\sqrt{\Theta}}{(2+\alpha)\tau_n} - \frac{6(1-e)^{\tau}n\sqrt{\Theta}}{\sqrt{\pi}} = 0 \qquad \text{2-49}$$

Making the variable substitution

$$H^2 = \Theta \qquad \text{2-50}$$

transforms this equation into

$$H'' + K H = 0 \qquad \text{2-51a}$$

where

$$K = \frac{5\pi \tau_0^2}{2(2+\alpha)\tau_n^2} - 3(1 - e) \qquad \text{2-51b}$$

Because gravity has been ignored, there is no limit to the amount of material which can be sheared. The problem can be reformulated at two parallel boundaries moving in opposite directions. The separation distance between the boundaries is 2L, and z=0 is centered midway between the boundaries. The boundary conditions now become:

$$U_m = U(L) = -U(-L) \qquad \text{2-52}$$

If K=0, then there is no (mechanical) heat flux through the boundaries, and equations 2-51 have solutions:

$$U' = \frac{U_m}{L} \qquad \text{2-53}$$

$$N = N_0 \qquad \text{2-54}$$

$$H = \frac{U_m}{L} \left(\frac{2+\alpha}{30(1-e)}\right)^{1/2} \qquad \text{2-55}$$

The flow is simple shear flow, with constant volume concentration, temperature, and shear rate. The stresses are

given by:

$$T_{xz} = \frac{F(U')^2(2+\alpha)^{\frac{3}{2}}(1+e)}{5\sqrt{30}(1-e)\pi} \qquad \text{2-56a}$$

$$T_{zz} = \frac{F(U')^2(2+\alpha)(1+e)}{30(1-e)} \qquad \text{2-56b}$$

where

$$F = \frac{N^2(2-N)}{(1-N)^3} \qquad \text{2-57}$$

These results are completely consistent with Bagnold's. The primary difference is that the empirical functions of concentration determined by Bagnold have been replaced by the analytic expressions of equations 2-56 and 2-57.

The stress ratio is also constant, and given by

$$\frac{T_{xz}}{T_{zz}} = \frac{\tau_\theta}{\tau_n} = \left(\frac{6(1-e)(2+\alpha)}{5\pi}\right)^{\frac{1}{2}} \qquad \text{2-58}$$

For the more general case of $K > 0$ equations 2-51 and boundary condition 2-52 have solutions

$$U = U_m \frac{\sin(\sqrt{K}z)}{\sin(\sqrt{K}L)} \qquad \text{2-59}$$

$$H = \frac{U_m(2+\alpha)\sqrt{K}}{5\sqrt{\pi}} \frac{\tau_n \cos(\sqrt{K}z)}{\tau_\theta \sin(\sqrt{K}L)} \qquad \text{2-60}$$

In order to determine the stress ratio it is necessary to specify the heat flux at the boundaries:

$$q(L) = -q(-L) \equiv Q \qquad \text{2-61}$$

where $q = -\kappa\theta' = \frac{-\tau_n}{\sqrt{\pi}}\frac{\theta'}{\theta}$ from equation 2-48 \qquad 2-62

From equations 2-60 and 2-61 :

$$Q = \frac{\tau_n^2 \, U_m \, 2(2+\alpha)K}{5\pi \, \tau_0} \qquad\qquad 2\text{-}63$$

, so τ_0/τ_n is given by:

$$2\frac{\tau_0}{\tau_n} = \frac{Q}{U_m} + \left(\frac{Q^2}{\tau_n^2 \, U_m^2} + \frac{24(1-e)(2+\alpha)}{5\pi}\right)^{\frac{1}{2}} \qquad 2\text{-}64$$

Expressing H and U in terms of Q, τ_n, and U_m gives:

$$U = U_m \frac{\sin(\sqrt{K}z)}{\sin(\sqrt{K}L)} \qquad\qquad 2\text{-}65$$

$$H = H_m \cos(\sqrt{K}z) \qquad\qquad 2\text{-}66a$$

$$\text{where } H_m = \frac{Q\sqrt{\pi}}{2\tau_n\sqrt{K}\sin(\sqrt{K}L)} \qquad 2\text{-}66b$$

and where K is defined by equation 2-51c. For $K>0$, Q is positive, indicating fluctuation energy is lost through the boundaries. Energy enters the flow as the moving boundaries do work on the mean flow. The energy is converted via granular collisions into fluctuation (kinetic) energy, which in turn is either dissipated into true heat or diffuses through the boundaries. From equations 2-40c and 2-46, for increasingly elastic (higher e) collisions, Q increases. Since less kinetic energy is dissipated during collisions, more is lost through the boundaries.

For $K< 0$, equation 2-51 has solutions:

$$U = U_m \frac{\sinh(\sqrt{K}z)}{\sinh(\sqrt{K}L)} \qquad\qquad 2\text{-}67$$

$$H = H_m \frac{\cosh(\sqrt{K}z)}{\cosh(\sqrt{K}L)} \qquad\qquad \text{2-68a}$$

$$\text{where } H_m = \frac{\sqrt{\pi}Q}{2\,\tau_n\sqrt{K}\,\tanh(\sqrt{K}L)} \qquad\qquad \text{2-68b}$$

These solutions correspond to the case where fluctuation energy is highly dissipated by granular collisions, and the boundary must act as a direct source of fluctuation energy.

Examples of the velocity, concentration, and temperature profiles are plotted for the cases of $K=0$, $K>0$, and $K<0$, in Figure 2-9.

For $K>0$, the temperature and shear reach their maximums at the center of the flow, where N is at its minimum. The collisions between relatively inelastic grains dissipate more energy than is available from the mean shear, so macroscopic heat must diffuse inward from the boundaries. For $K<0$, the situation is the opposite: collisions between highly elastic grains generate more fluctuation energy than they dissipate, so macroscopic heat diffuses outward towards the boundaries.

At this point it is useful to consider the function $\alpha(N)$ which parameterizes the collision anisotropy discussed earlier. As mentioned, the theory of Savage and Jeffrey(1981) is consistent with that of Jenkins and Savage(1983) for the case where the precollisional velocity fluctuation is large compared to the mean velocity. Savage

and Jeffrey derive the anisotropy function to be

$$A = \text{erfc}\left(\frac{\bar{K}\cdot\bar{U}}{\sqrt{\Theta}}\right) \hspace{3cm} \text{2-69a}$$

where

$$\text{erfc}(x) = \frac{2}{\pi}\int_x^\infty e^{-t^2}\,dt = 1-\text{erf}(x) \hspace{2cm} \text{2-69b}$$

$$= 1 - \frac{2}{\sqrt{\pi}}\,e^{-x^2}\sum_{n=0}^\infty \frac{2^n x^{2n+1}}{1\cdot 3\cdots 2n+1}$$

Assuming the argument is small, a linear form is adopted for erfc(x) retaining only the first term in $\bar{K}\cdot\bar{U}/\sqrt{\Theta\pi}$

$$A = 1 - 2\,\frac{\bar{K}\cdot\bar{U}}{\sqrt{\Theta\pi}} \hspace{3cm} \text{2-69c}$$

In this approximation we find $\alpha = 2$. Although $\bar{K}\cdot\bar{U}$ is not always much less than $\sqrt{\Theta\pi}$, this approximation gives some idea of the order of magnitude of α.

Using a value of $\alpha = 5$, τ_0/τ_n can be calculated from equation 2-58 for the gravity free shear flow discussed earlier. For glass grains, e is approximately 0.9, giving:

$$\frac{\tau_0}{\tau_n} = \frac{6(1-.9)(2+5)}{5\pi} = 0.52 \hspace{2cm} \text{2-70}$$

This value is close to measurements of the stress ratio to be discussed is section 4.

2.4.2.2 Numerical solutions using 'kinetic' theory

Returning now to the semi-infinite granular bed described earlier, equations 2-45 and 2-46 can be combined
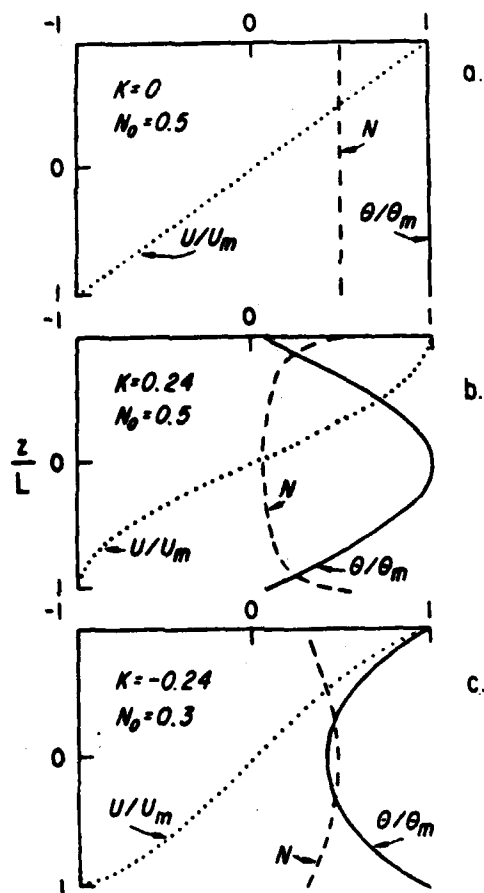
Figure 2-9. Analytic solutions for the velociy, volume concentration, and pseudo-temperature based upon the constitutive theory of Jenkins and Savage (in the limit of g → 0). Values are normalized by the maximum values. a) no heat flux through the boundary, b) heat flux out of the material(K>0), c) heat flux into the material(K<0).

and simplified by redefining κ as:

$$\kappa \equiv cF\sqrt{\Theta} \qquad\qquad\qquad \text{2-71a}$$

$$\text{where } c = \frac{1+e}{\sqrt{\pi}} \qquad\qquad\qquad \text{2-71b}$$

$$\text{and } F = \frac{N^2(2-N)}{(1-N)^3} \qquad\qquad\qquad \text{2-71c}$$

By introducing the definition:

$$I = \Theta' \qquad\qquad\qquad \text{2-72}$$

the following equations are obtained:

$$F' = \Theta^{-1}\left(\frac{N}{c\sqrt{\pi}} - FI\right) \qquad\qquad\qquad \text{2-73}$$

$$I' + I\left(\frac{F'}{F} + \frac{I}{2\Theta}\right) + \frac{5\tau_\Theta^2}{(2+\alpha)c^2F^2\Theta} - 6(1-e)\Theta = 0 \qquad \text{2-74}$$

$$U' = \frac{-5\tau_\Theta}{(2+\alpha)cF\sqrt{\Theta}} \qquad\qquad\qquad \text{2-75}$$

Equations 2-73 to 2-75 can be numerically integrated with the application of appropriate boundary conditions (equation 2-47) at the upper surface of the flow. As mentioned earlier, the energy flux through the boundary and hence boundary condition for Θ' is not well understood. For this reason solutions are presented for both boundary conditions 2-47d and 2-47e.

Some examples of the numerical solutions for U, N, and Θ are given in Figure 2-12. In this figure, $\alpha = 5$ and $e = 0.9$. The integration was stopped at a depth of ten grain diameters.
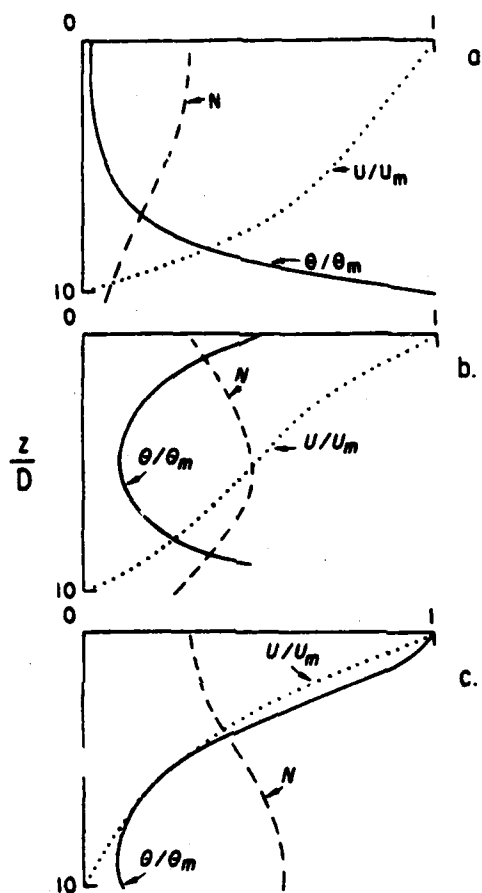
Figure 2-10. Numerical solutions for the velocity, volume concentration, and pseudo-temperature based upon the constitutive theory of Jenkins and Savage. The velocity and pseudo-temperature are normalized by their maximum values. Depth in the bed is nondimensionalized by the grain diameter. In all solutions $\alpha=5$. For a): $\tau_0=5, \tau_n=10, \Theta'=0$ at $z=0$; b): $\tau_0=5$, $\tau_n=10$, $\Theta'=-D(U')^2$ at $z=0$; c): $\tau_0=5.8, \tau_n=10$, $\Theta'=0$ at $z=0$.

As illustrated earlier in the analytic solutions, there is a positive correlation between U' and θ , and a negative correlation between U' and N. The first condition arises because the mean shear is the source of energy for velocity fluctuations. The second correlation simply reflects the dilatent behavior of granular materials.

Figures 2-10a and 2-10b illustrate that the nature of the flow depends upon the stress ratio and energy flux at the upper boundary. With $\theta'=0$ and N_o kept constant, a high value of $\dfrac{\tau_o}{\tau_n}$ results in (Figure 2-10c) N increasing with depth, while U' and θ decrease with depth. A lesser $\dfrac{\tau_o}{\tau_n}$ (Figure 2-10a) results in the opposite trends.

This is explained by examining the amount of energy converted from the mean shear into fluctuation energy, relative to the amount of energy dissipated in the collisions. Taking the ratio of these two quantities (from equations 2-74 and 2-75) gives

$$\Delta E = \frac{(2+\alpha)(U')^2}{30(1-e)\theta} = \frac{5\tau_\theta^2}{6(1-e)(2+\alpha)c^2F^2\theta^2} \qquad 2\text{-}76$$

If $\Delta E \neq 1$, then in order to conserve energy, there must be a vertical diffusion of fluctuation energy. Rewriting ΔE in terms of the applied stresses it is found that at the upper boundary:

$$\Delta E\Big|_{z=0} = \frac{5\pi}{6(2+\alpha)(1-e)}\left(\frac{\tau_\theta}{\tau_n}\right)^2 \qquad 2\text{-}77$$

If ΔE is greater than 1 (high $\dfrac{\tau_o}{\tau_n}$), then there is an excess of fluctuation energy which diffuses downward into

the material. As a consequence, the pseudo-temperature and shear must decrease with depth, and the concentration must increase, as seen in Figure 2-10c. If ΔE is less than one, then the opposite effects must occur, as in Figure 2-10a. Figure 2-10b demonstrates that a low stress ratio at the boundary can be compensated for by allowing the boundary to act as a source of fluctuation energy ($\Theta' < 0$).

It is interesting to note that ΔE is proportional to the stress ratio (see equation 2-30c), and must therefore decrease with depth as a consequence of the self-weight of the grains. Eventually ΔE will reach a value less than one, and fluctuation energy will have to be conducted into this region. For any given flux at the surface, there is a finite depth to which the energy can be conducted, since it will continually be lost (below the depth where $\Delta E = 1$). At this depth the pseudo-temperature will be at its minimum. Below this depth, the energy conservation equation can only be satisfied if there is a source of energy somewhere below.

This is unreasonable for the semi-infinite granular bed, so it must be assumed that the equations of motion are no longer valid below the maximum depth toward which fluctuation energy can diffuse. Physically, this is due to the concentration increasing and the pseudo-temperature decreasing to such an extent that the grains are 'frozen' into a rigid packing. This depth is clearly analogous to the level of no motion, but in the context of this theory, it is the depth at which $\Theta' = 0$, or the level of 'thermalization'.

3.   Experimental considerations

An apparatus capable of measuring the large stresses
and dilatency effects typical of granular-fluid materials
undergoing rapid shear deformation was constructed in order
to experimentally study the validity of a dynamic yield
criterion and evaluate the constitutive theories of section
2.3.

The granular materials chosen for study in this
apparatus were spherical glass beads and natural sand. In
accordance with the theoretical developments previously
presented, the majority of the experiments involved the
shearing of spherical glass beads in air. However, because
many granular flows of interest involve nonspherical grains,
and immersing fluids with densities comparable to that of
the grains, series of experiments were also run using water
as the immersing fluid, and sand as the granular material.

3.1 Apparatus

An annular, parallel plate shear cell, sometimes
called a ring, annular ring, or torsional shear cell, is
shown schematically in Figure 3-1. The design closely
follows that of Carr and Walker (1868), and Savage (1978).
The primary modification is that the outer wall is clear,
allowing for direct visual observations.
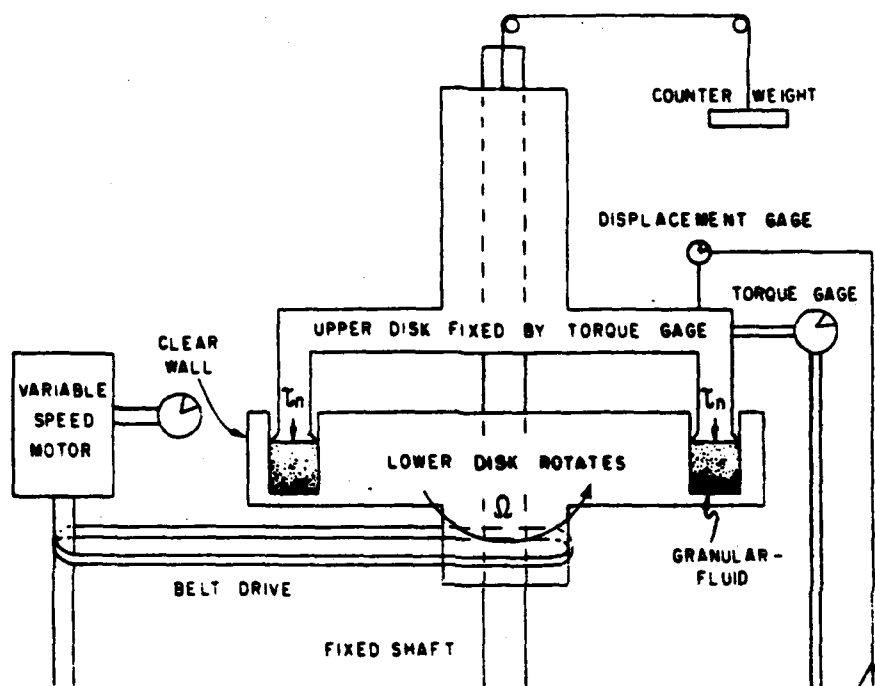
Figure 3-1.   Schematic of annular shear cell apparatus.

Shearing takes place in a 4.4 centimeter wide annular gap centered at a radius of 12.4 centimeters. The area of a horizontal slice through the annulus was 341 square centimeters. The at rest volume of the material studied ranged from about 200 to 1000 cubic centimeters.

The upper and lower plates were roughened by cementing with epoxy one to two grain layers of the material being sheared to each surface. The side walls were smooth, and rotated rigidly with the lower plate, which was belt driven by a variable speed motor. The upper plate was free to move vertically, but restrained from rotating by a linkage to a strain gage. A counterweight system allowed variation of the applied normal stress.

The outer wall was clear acrylic, protected by a thin, replaceable, clear polycarbonate inner lining. This allowed for direct visual observation of the boundary between the shearing and nonshearing regions, when such a boundary existed.

For any given experiment the independent variables were: the applied normal stress, τ_n; the rotation rate of the bottom plate with its annular ring; and total mass of the granular-fluid material. The measured dependent variables were: the force exerted by the upper plate on the strain gage, F; the displacement of the upper plate; and the location of the boundary between the shearing and nonshearing regions, if it existed. Calculated variables include: the normal stress at the boundary between the

shearing and nonshearing regions (from eq. 2-8b); the mean
shear stress, τ_o,(from eq. 4-2); the average, or nominal
volume concentration in the shearing region, N, defined as
the mass of material in the region divided by the volume of
the region; and the nominal shear rate, defined as the
difference in velocity between upper and lower plate divided
by the thickness of the shearing region.

3.2 Material description

The granular materials used in this study were
spherical glass beads and natural sand. The sand was
obtained from Boomer Beach in La Jolla, California. The
sand is a well rounded, quartz sand, and is described by
Inman(1953). The sand was washed and sieved into the size
fraction which was used in the experiments. The upper and
lower sieve mesh sizes were .594 mm and .500 mm, giving the
sand a nominal diameter of .55 mm. The glass beads were
purchased from Potters Industries of New Jersey and the
Ferro Corporation of North Carolina. Because the beads had
a large variation in the degree of their sphericity, only
the most spherical grains were used. These grains were
separated from the less spherical ones by rolling them down
a smooth plane inclined at approximately two degrees from
horizontal. The beads were also sieved to obtain nearly
uniform sizes. The upper and lower mesh sizes for the
nominal 1.1 mm spheres were 1.189 mm. and 1.0 mm. The upper

and lower mesh sizes for the nominal 1.85 mm spheres were
2.0 mm and 1.7 mm.

The densities of the various materials were
determined by measuring the amount of water displaced in a
100 ml. graduated cylinder by a known mass of material.

The physical characteristics of the materials are
given in Table 3-1.

3.3 Experimental plan

Given three different materials and two immersing
fluids, there were six possible combinations of granular
material and interstitial fluid. Depending upon the amount
of material and the conditions to which it was subjected,
two types of flow were observed. In one case, all of the
material in the annulus sheared. In the second case, only
a portion of the material sheared, while the rest of the
material remained locked in rigid body rotation below the
shearing grains. These two cases are referred to as fully
and partially shearing. The differences between them will
be discussed in section 4. For each type of flow, the
applied normal stress and the velocity of the lower boundary
could be independently controlled, as described above.

The basic procedures for the experiments are as
follows:

A pre-weighed amount of granular material was placed
in the shear cell. For the partially shearing experiments,

Material	Nominal Diameter (mm)	Density (gm/cm^3)
Spherical glass beads	1.1	2.5
	1.85	2.8
Natural, well rounded quartz sand	0.55	2.6

Table 3-1. Characteristics of the granular materials.

chalk dust was placed on the side wall. After applying a known normal stress, the material was pre-stressed and consolidated by slowly shearing it back and forth for five cycles. The initial at rest volume of the material was recorded along with the zero offset of the strain gage. The shearing was begun by slowly increasing the speed of rotation of the bottom assembly to the desired level. After steady state was reached (about 5-15 seconds), the period of rotation, the output of the strain gage, and the displacement of the upper plate were recorded. The motor speed was then reduced slowly to zero. The level of no motion was recorded for the partially shearing experiments by measuring where the chalk dust had been rubbed off of the side wall. The material was then post-stressed and consolidated as before. The final at rest volume of the granular material and the zero offset of the strain gage were recorded again. If these values deviated from the initial values, then the averages of the two were used in later calculations.

The entire process was repeated for a variety of applied normal stresses and speeds. For the fully shearing experiments the speed was adjusted to maintain the same volume concentration over a range of applied normal stresses. For these experiments, the normal stress and the associated speeds of rotation were changed without bringing the system to a halt after it was determined the results thus obtained were the same as when the shearing was stopped

after each run.

For the experiments in which water was the
interstitial fluid, water was added to the system as the
material dilated. This was done in order to maintain the
fluid level even with the surface of the upper plate, and
thus avoid any buoyancy effect on the plate (which would
introduce uncertainty in the applied normal stress).

3.4 Measurment systems

The variables which were directly measured were the
mass and the initial, at rest volume of the granular
material, the change in volume of this material during
shear, the torque transmitted by the granular material from
the lower rotating plate to the upper fixed plate, the
rotational period of the lower plate and attached side
walls, and the thickness of the shearing region while shear
was occuring and afterwards, when it was at rest.

The total mass of the granular material was measured
using a pan balance accurate to 0.1 grams. The at rest
volume of this material was calculated from measurements of
the height of the material in the annulus of the shear
apparatus. The resolution of this measurement was 0.05
centimeters, corresponding to a volume of 17 cubic
centimeters. The change in volume during shearing was
calculated by measuring the vertical displacement of the
upper plate with a machinist's gage accurate to 0.0013

centimeters. Note that this measurement was made without stopping the rotation. The torque exerted on the upper plate was measured be means of a strain gage mounted on a steel beam. This instrument, with its associated electronics, produces a signal linearly proportional to the transverse force applied to the beam. A calibration curve is shown in Figure 3-2. As seen, the instrument is quite linear, with a correllation coefficient of 0.99996. The mechanical linkage between the shear apparatus and the strain gage is shown schematically in Figure 3-3. Referring to Figure 3-3, the force applied to the strain gage beam, F, is:

$$F = \text{Torque} \times R \qquad\qquad 3-1$$

where:

$$\text{Torque} = \int_{r_1}^{r_2} T_{xz}(r) 2\pi r \, dr \qquad\qquad 3-2$$

In performing this calculation .t was assumed $T_{xz}(r)$ was constant across the annular gap for a given experiment. If, in fact, $T_{xz}(r)$ was a linear or quadratic function of r, the assumption of a constant T_{xz} results in errors of 2 and 4 per cent, respectively, for T_{xz} at the mean radius. The resolution in measuring T_{xz} was 0.001 volts, corresponding to approximately 10 dyne/cm² for T_{xz}.

The speed of rotation of the lower plate, and hence the maximum velocity, was measured by a frequency counter coupled to a magnetically actuated switch. A magnet was attached to the rotating disk. Each time the magnet passed the switch, the counter triggered and counted the time until
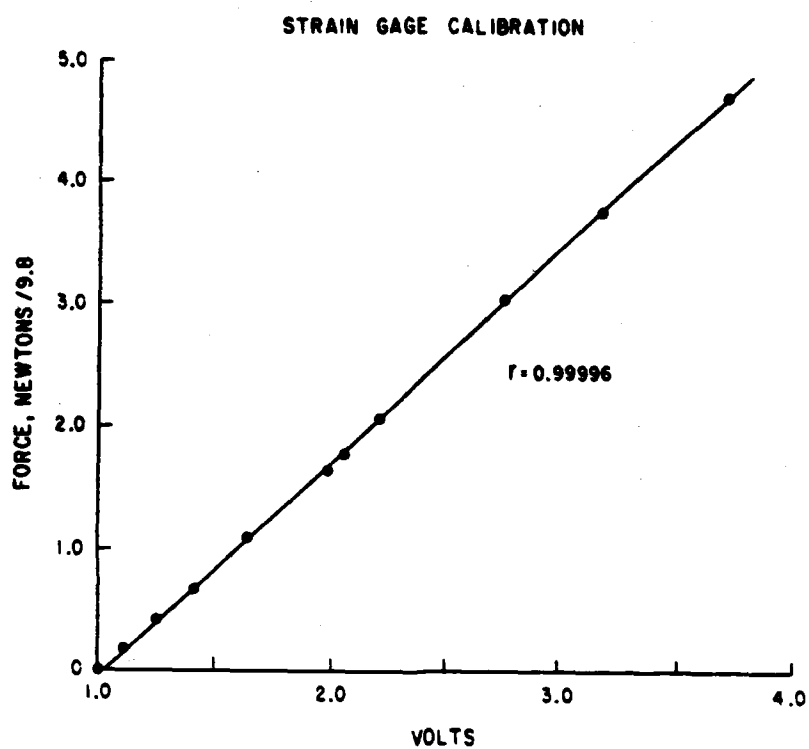
Figure 3-2.   Strain gage calibration curve.

R=18.2 cm

TORQUE

UPPER

PLATE

STRAIN GAGE
LINKAGE

F = TORQUE x R
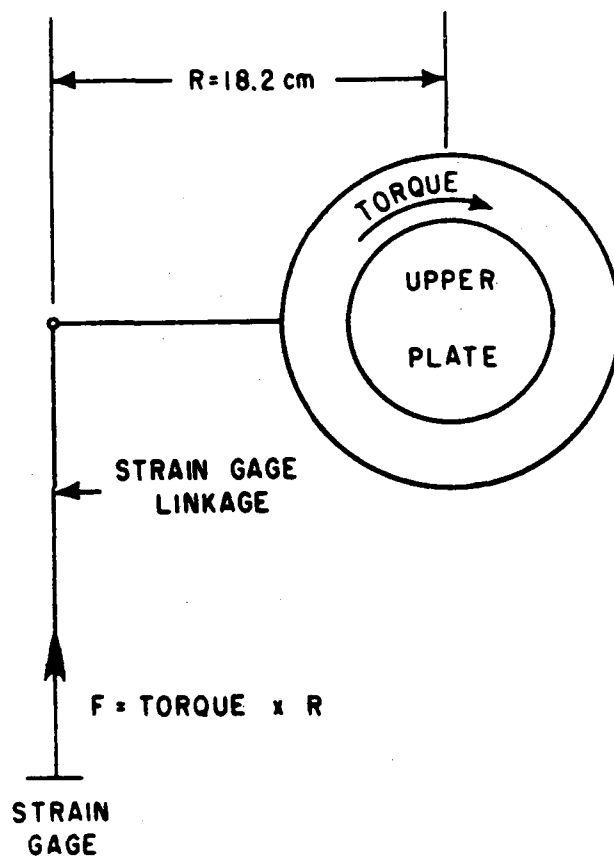
STRAIN
GAGE

Figure 3-3.   Plan view of linkage to strain gage.

The force measured by the gage is equal to the torque
exerted by the upper plate times the moment arm, R.

the next trigger. The accuracy of this method was 0.001 seconds, corresponding to a speed resolution of 0.1 cm/sec.

In order to visually record the thickness of the shearing region, the outer wall of the apparatus was made of clear plastic. The method used was to apply chalk dust to a section on the inside of the outer wall. The shearing grains wiped the chalk dust off the wall, while the nonshearing grains left the chalk dust unaltered. The method was verified by placing columns of dyed grains at various positions inside the annulus and, subsequent to shearing, excavating to examine for the depth at which the column of dyed grains remained intact. Both methods gave the same results, indicating the side wall effects were probably quite small for this type of flow. The resolution of this method was approximately one grain diameter.

The accuracies of all of these measurement systems are summarized in Table 3-2. The accuracies are also expressed as a fraction of a typical measurement.

3.5 Approximations and assumptions

In attempting to experimentally study the flow described in section 2 there are several assumptions made and approximations used. The primary areas of concern are the effects of rotation, the local influence of the side wall boundaries, the effects of the interstitial fluid, and unsteadiness in the flow.

Measurement	Resolution	Accuracy %
Mass of granular material	0.1 gram	0.001
Displacement of upper plate	0.0013 cm	1.7
Location of internal boundary	0.05 cm	1.25
Shear stress	10 dyne/cm^2	0.2
Normal stress	70 dyne/cm^2	1.4
Nominal shear rate	0.5 cm/sec	1.4
Nominal volume concentration	0.017	3.8

Table 3-2. Maximum errors in the measurement systems.

3.5.1 Effects of rotation

The flows considered in section two were purely two dimensional, that is, there was no dependence upon the cross stream direction. The experimental apparatus, however, because of its rotational nature, introduces the possible complications of radial dependence of the field variables. The two most worrisome complications are centrifugal effects, and a non-uniform shear rate across the gap.

The tendency for a non-uniform shear rate is reduced by decreasing the ratio of the width of the annular gap to its mean radius. For this apparatus the ratio was 0.35, giving a maximum deviation in velocity from that at the mean radius of 15 percent. It would have been desirable to either reduce the width of the annular gap or increase the mean radius. Unfortunately, both of these options were precluded by other considerations. The gap width could not be further reduced because a narrower gap would limit the number of grains in the cross flow direction to such a small number that the continuum assumption would be questionable. Furthermore, since it was unknown whether or not the side walls influence the local flow, it was desirable to have as wide a gap as possible to minimize such effects on the overall flow. The mean radius could not be increased because the funds available were insufficient to cover the costs of manufacturing a larger unit.

The effects of radial accelleration, or so called centrifugal effects, were always present to some extent, but rotational speeds and applied normal stresses were selected to insure that the centrifugal stress was always much less than the normal stress. This imposed an upper limit on the maximum velocity for each applied normal stress. This limit is shown in Figure 3-4, where the centrifugal stress is 25 percent of the normal stress.

Savage and Sayed (1983) measured secondary (radial) flows of granular-fluid materials in a nearly identical apparatus. They concluded these flows were quite small compared with the primary flow, and did not effect the stress measurements.

Since the interstitial fluid does not support an anisotropic normal stress, the centrifugal forces could have a significant upon the dynamics of the interstitial fluid. This will be discussed futher in section 3.6 on data quantity and quality.

3.5.2 Boundary wall effects

The mechanics for stress transfer at a solid wall boundary are probably different from those in the interior of the flow, because the wall is relatively massive and unmovable compared to a grain. In fact, the influence of the boundary is expected to be related to its surface roughness, as well as its rigidity. For a rough boundary,
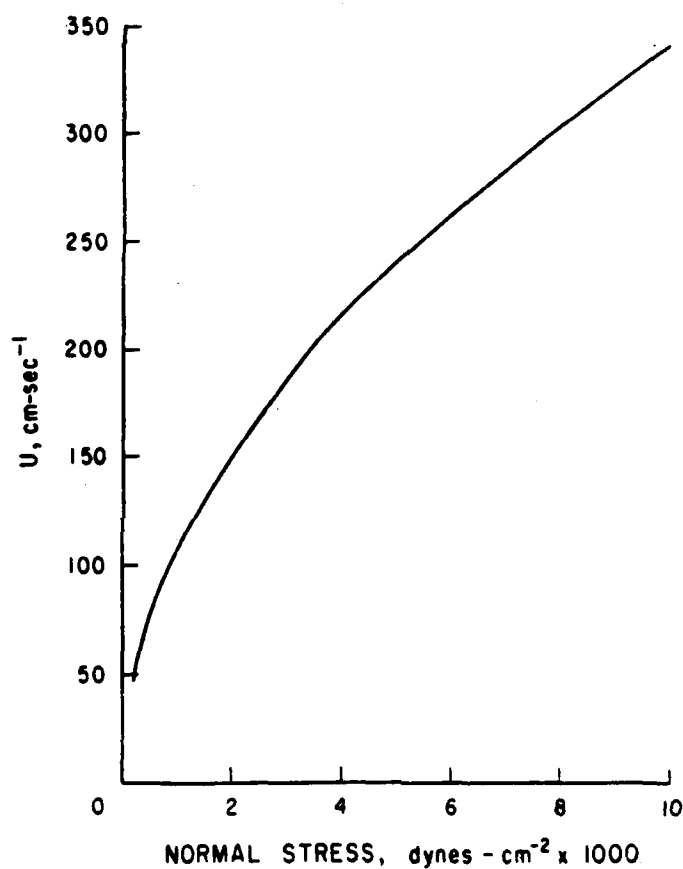
Figure 3-4. The velocity at which the centrifugal stress is 25% of the normal stress is plotted as a function of the normal stress, for D=1.1mm, and $\rho_s = 2.5$ gm/cm^3.

one might expect the traditional "no slip" condition to be
valid. But at a smooth boundary it is much more likely that
slip occurs between the wall and the nearest grains. In this
case a "no stick" condition may be more appropriate. The
distinction between the no slip and no stick conditions
depends upon the frictional nature of the granular-fluid
material and the wall material.

For these experiments the side walls were smooth
aluminum and smooth polycarbonate, both coated with a thin
layer of teflon. The upper and lower boundaries, on the
other hand, were roughened with one to two layers of the
granular material being studied.

It is assumed that the side walls are slippery, and
the upper and lower shearing surfaces do not allow slip.
Thus the boundary conditions applied at the top and bottom
of the flow are that the flow velocities approach the
boundary velocities. The validity of the assumption that
the side wall is slippery is supported by the measurements
of the thickness of motion which were discussed in the
previous section.

3.5.3 Interstitial fluid effects

As discussed in section 2, the effects of the
interstitial fluid on the dynamics of rapidly flowing
granular-fluid materials have been assumed to be negligible.
The validiy of this seemingly gross assumption can be judged

by considering the work of Bagnold(1954). Bagnold found
that for granular concentrations greater than approximately
10 per cent, the granular-fluid resistance to shear was
always much greater than the viscosity of the purely fluid
phase. Bagnold separated the behavior of a granular fluid
into two limiting cases, the macro-viscous regime, and the
grain-inertia regime.

In the macro-viscous regime, stresses are
transmitted by interstitial fluid friction, and are
therefore dependent upon the fluid viscosity. In the grain-
inertia regime, stresses are transmitted by intergranular
collisions and are independent of the fluid viscosity. The
Bagnold number, defined by equation 2-15, and representing
the ratio of the inertial to the viscous forces, can be used
to characterize the flow as either viscous, collisional, or
intermediate. Bagnold found that for B <40 the flow is
entirely in the macro-viscous regime, and for B>450 it is in
the grain-inertia regime. Bagnold refers to the region
between ranges as the transition region.

In the present experiments, granular concentrations
are always greater than 0.2. Bagnold numbers can be
computed based upon mean granular concentration and nominal
shear rates. These numbers are given in Table 3-3 .
Clearly all the flows involving air as the immersing fluid
are in the grain inertia regime. On the other hand, flows
involving water as the interstitial fluid range from the
transitional to the grain inertia regimes, as will be shown

Bagnold numbers

In air   14,000-161,000

In water

   1.1 mm spheres

    fully shearing   348-2500

    partially shearing   273-882

   1.85 mm spheres

    fully shearing   870-3422

    partially shearing   .247-1186

   0.55 mm sand   280-666

   partially shearing

Table 3-3. Range in Bagnold numbers for the various
       sets of experiments, where :

$$B = \rho_s D^2 \lambda^{\frac{1}{2}} \frac{dU}{dz} / \mu$$

   For B>450, the data lie in the grain inertia region.

in section 4.

3.5.4 Unsteadiness

In general, the flows reached a steady state after
a few seconds of shearing. However, there were two
identifiable sources of unsteadiness. The first resulted
from an imperfectly designed apparatus, the second is
believed to be a consequence of the mechanics of deformation
of some granular-fluid materials.

The first source of unsteadiness was the insertion
of a grain or grain fragment between the fixed upper plate
and the rotating side wall. This caused a temporary jamming
of the apparatus, and a subsequent "ringing" type of
behavior after the grain was fractured or dislodged. If
this behavior was observed, the experiment was stopped, the
grain fragment removed(if it could be found), and the
experiment repeated.

The second observation of unsteadiness resembled a
"stick-slip" behavior, and occured at low shear rates. When
this behavior occured, the rotation rate alternately slowed
down and speeded up. This sort of behavior has been
reported by Cheng and Richmond (1978) for suspensions of
grains, but it is not completely understood. In the present
experiments, it is believed this behavior results when the
material alternately dilates and compresses, causing a
decrease or increase in the material's resistance to shear.

This behavior was observed for glass spheres only near the threshhold stress for initial yield. For sand, however, the behavior was observed from the yield point up to shear rates of approximately 40 seconds^{-1}. Presumably this is related to the angularity of the sand, and the preferred orientation, or fabric, which the material develops during shearing. This interesting phenomenon merits future study, but since it complicates the interpretation of the steady flow problem, the shear rates were restricted to avoid this unsteady complication.

3.6 Quantity and quality of data

A summary of the quantity of the various experiments is given in Table 3-4. In general, the experiments involving glass spheres were consistent and repeatable. These data reveal clear trends and form the basis of most of the discussion in the next section.

In contrast, the experiments on sand, and those on 1.1 mm glass spheres with water, were less consistent. Due to both a lack of foresight and financial restrictions, the shear cell was designed to study only those granular-fluid materials having diameters ranging from 0.5 mm to 3 mm. Natural beach sand, being somewhat angular, has some cross sections much less than .5 mm. In order to prevent the sharp edges of the sand grains from jamming into the gap between the Delrin lip and the side wall (see Figure 3-1), the

Delrin was replaced with a tighter fitting and more durable
stainless steel lip. This worked satisfactorily for dry
sand, but caused a secondary problem for the wet
experiments. Normally when shearing begins, the granular-
fluid material dilates and the upper plate moves upward.
Air or water flows downward between the lip of the upper
plate and the side wall to fill the voids created between
the grains. For the experiments on wet sand, water could
not flow freely between the stainless steel lip and the
replaceable polycarbonate lining on the inside of the outer
wall. The result was that the lining deformed, creating a
tight seal with the steel lip. This caused a pressure
deficit within the granular-fluid material, and prevented
any dilation. This introduced a great uncertainty in the
value of the normal stress, and lesser uncertainties for the
shear stress and volume concentration. This set of
data(sand-water) must be considered to be of very poor
quality, and therefore of little value in evaluating the
constitutive behavior or the yield criterion.

Experiments on sand in air had similiar problems
related to the frictional nature of angular, quartz grains.
The interaction with the side wall was frictional, so the
'slippery' boundary condition at the side walls is suspect.
The measurents of the shear stress could have been biased by
this effect, since stress could be transferred from the side
walls to the granular material.

The second set of experiments in which the quality
is suspect involves the full shearing of 1.1 mm glass
spheres in water. In order to fully shear the material the
minimum depth of the annular gap had to be decreased by
raising the lower boundary. This was done by inserting into
the annulus a 2 cm thick plexiglass toroid. This insert
could have had some subtle effects upon the flow. For
example, if the toroid surface was not exactly parallel to
the upper plate, then the material would be forced to
alternately compress and dilate. A second problem for this
set of experiments could be the effect of radial forces on
the interstitial fluid. Although the centrifugal forces
were small compared to the intergranular forces, they were
large compared to the interstitial fluid pressure. In
response to the centrifugal force, the fluid should flow
outward to develop a radial pressure gradient as seen in
Figure 3-5 . This could have provide some bouyancy to the
upper plate, and consequently some error in the normal
stress calculation. Furthermore, it is possible as air gap
existed in the shearing region as shown in Figure 3-5. For
these reasons, this data set should be regarded with some
suspicion.

In summary, the 124 experiments involving glass
spheres in air, the 29 experiments involving 1.85 mm glass
spheres in water, and the 10 partially shearing experiments
involving 1.1 mm glass spheres in water are thought to be of
good quality. The 41 experiments involving sand and the 18
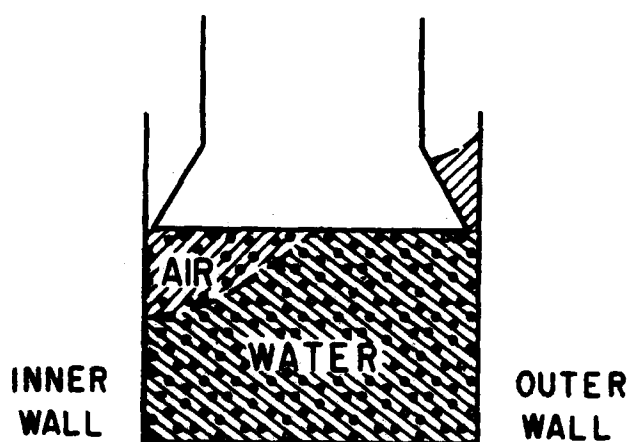
Figure 3-5.   A possible effect of rotation on the
interstitial fluid would be to create an air pocket near the
inner wall.

fully shearing experiments involving 1.1 mm glass spheres in water are of lower quality.

	Number of Experiments	Range in N
In Air		
1.1 mm fully shearing	36	0.37-0.56
1.1 mm partially shearing	50	0.29-0.61
1.85 mm fully shearing	18	0.44-0.49
1.85 mm partially shearing	20	0.30-0.53
0.55 mm sand	22	0.43-0.58

<div align="center">subtotal   146</div>

In Water		
1.1 mm fully shearing	18	0.55-0.58
1.1 mm partially shearing	10	0.64-0.67
1.85 mm fully shearing	12	0.50-0.51
1.85 mm partially shearing	17	0.50-0.53
0.55 mm sand	19	0.56-0.59

<div align="center">subtotal   76</div>

<div align="center">total 222</div>

Table 3-4. Summary of the number of experiments of each type, and the range in volume concentrations in the experiments.
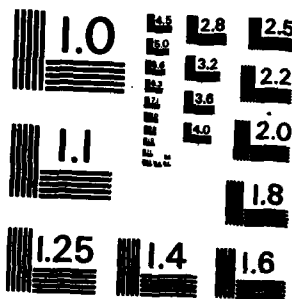
MICROCOPY RESOLUTION TEST CHART

NATIONAL BUREAU OF STANDARDS-1963-A

4. Results and discussion

The experimental results have application to several
aspects of granular-fluid flow, including the constitutive
behavior, and the applicability of a dynamic Coulomb yield
criterion in predicting the location of the boundary between
shearing and nonshearing grains. These data can also be
examined with regard to the differences between fully
shearing flows and flows in which there is an internal
boundary separating shearing and nonshearing regions
(partially shearing flow). Lastly, effects of the
interstitial fluid, and an effect of grain shape are
suggested by the experimental observations.

The data support the concept that the stresses are
nonlinearly dependent upon the shear rate, for flows in
which the effects of the interstitial fluid are negligible.
The stresses were found to be weakly dependent upon the
volume concentration up to approximately 0.45. Above this
concentration the stresses were found to be strongly
dependent on the volume concentration. These results are
consistent with Bagnold's (1954) measurements, although the
material constants are slightly different. The theory of
Jenkins and Savage(1983) correctly predicts the dependence
of the stresses upon the shear rate. Their predicted
functional dependence of the stresses upon the volume
concentration has the proper trend, but it underpredicts the

stresses for volume concentrations greater than
approximately 0.5, unless the influence of the volume
concentration on the collision anisotropy is empirically
determined from the data.

The stress ratios were found to be approximately
constant, with a weak dependence upon the shear rate, and
the volume concentration. The application of a dynamic
Coulomb yield criterion appears to be valid, although there
is significant spread in the data related to the immersed
weight of the moving grains.

The stress ratios measured for the fully shearing
flows were found to be consistently higher than those
measured for the partially shearing flows. Flows in water
tended to have higher stress ratios than flows in air,
possibly because of the effects of fluid viscosity.
Observations that prior flow history affects the subsequent
yield for experiments involving sand suggest that angular
grains develop a preferred fabric during shearing.

4.1 Constitutive behaviour

The constitutive behavior for the fully shearing
experiments is well defined because in these experiments the
volume concentration and the shear rate were varied
separately. This makes it possible to independently assess
the influence of either variable upon the stress state.

The shear stress and the normal stress are shown as a function of the nominal shear rate, U_m/Z_o, in Figures 4-1 to 4-2. As expected, the stresses are increasing functions of both the volume concentration and the shear rate.

The 1.1 mm glass spheres in air have the curious behavior that the stress appears to be nearly independent of the volume concentration for $N<0.45$. Savage(1978) observed the same phenomenon, and explained it as resulting from an air gap in the shearing region. Although no such gap was observed for the present experiments, it is possible one existed internally, as diagramed in Figure 4-3.

According to the collision theories discussed in section 2.3, the stresses should have a quadratic dependence upon the shear rate. In Figures 4-4 and 4-5 the natural logarithm of the shear stress (or normal stress) is plotted against the natural logarithm of the shear rate for the same experiments shown in Figures 4-1 and 4-2. In the experiments for which air is the interstitial fluid, the slopes (for constant N) are approximately 2, supporting the predicted quadratic relationship. For the experiments in which water is the interstitial fluid, the slopes vary between 1 and 2. This is consistent with earlier calculations showing that some of these experiments lie in Bagnold's transition regime, where fluid stresses play an important role. The open points in Figure 4-5 indicate the data are in the transition region. In terms of the kinetic
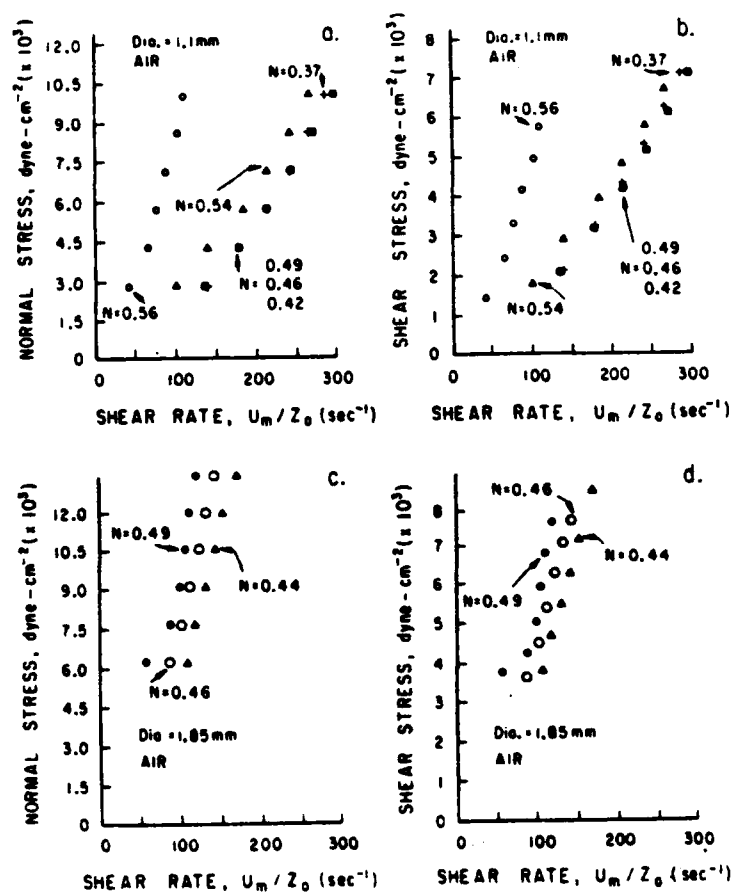
Figure 4-1. Stresses vs shear rate for glass spheres in air. Note the lack of dependence on the volume concentration for N<.5 (for the 1.1 mm spheres).
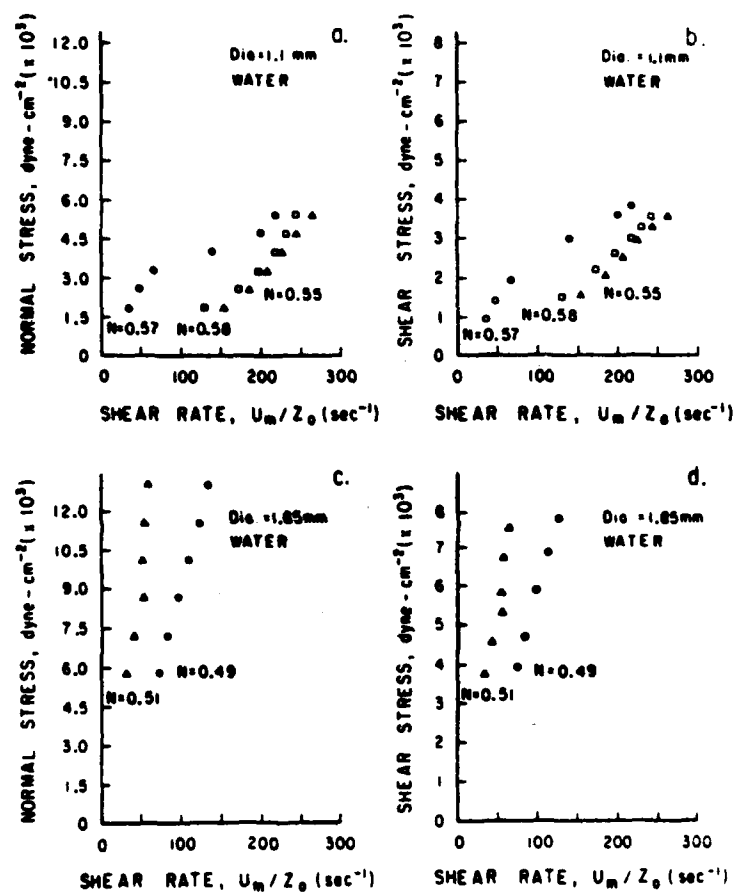
Figure 4-2. Stresses vs shear rate for glass spheres in water. The open circles indicate data with Bagnold numbers less than 450.
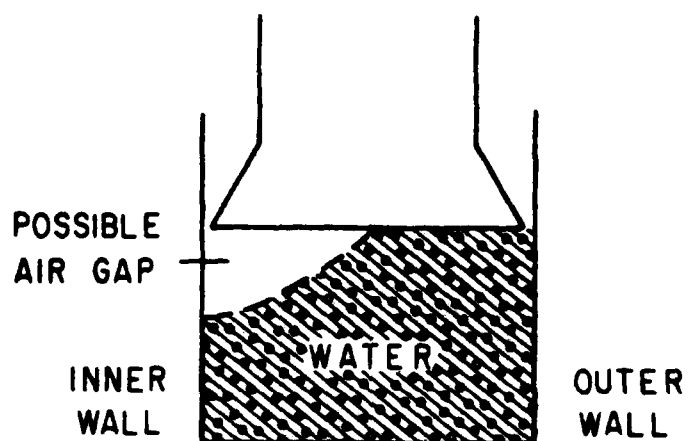
Figure 4-3. Schematic of an gap in the granular material which may have formed at high shear rates and low volume concentrations.
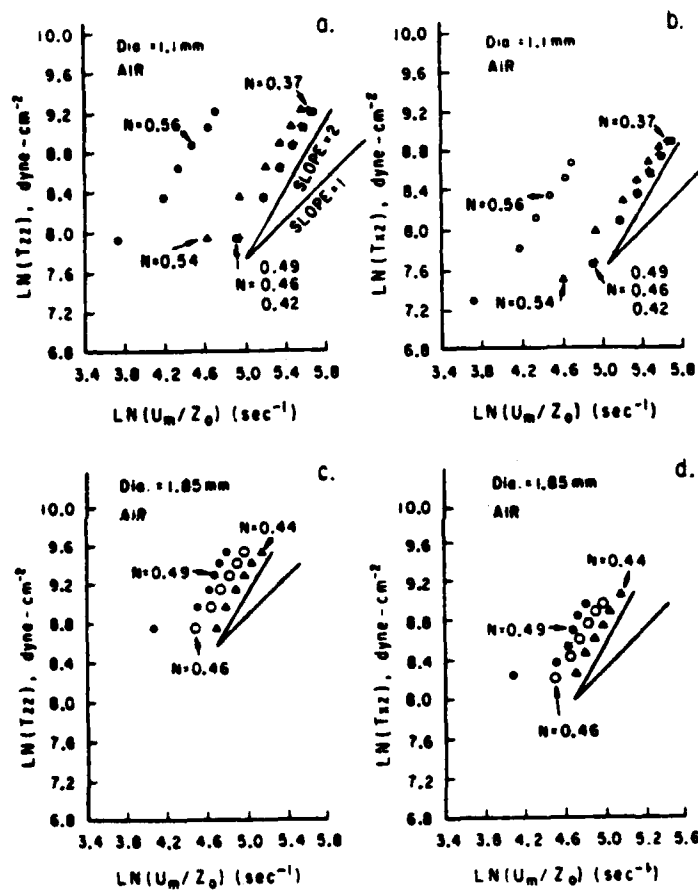
Figure 4-4. Ln stress vs ln shear rate for glass spheres in air (same data as Figure 4-1). A slope of two (at constant N) indicates a quadratic dependence of the stresses upon the shear rate.
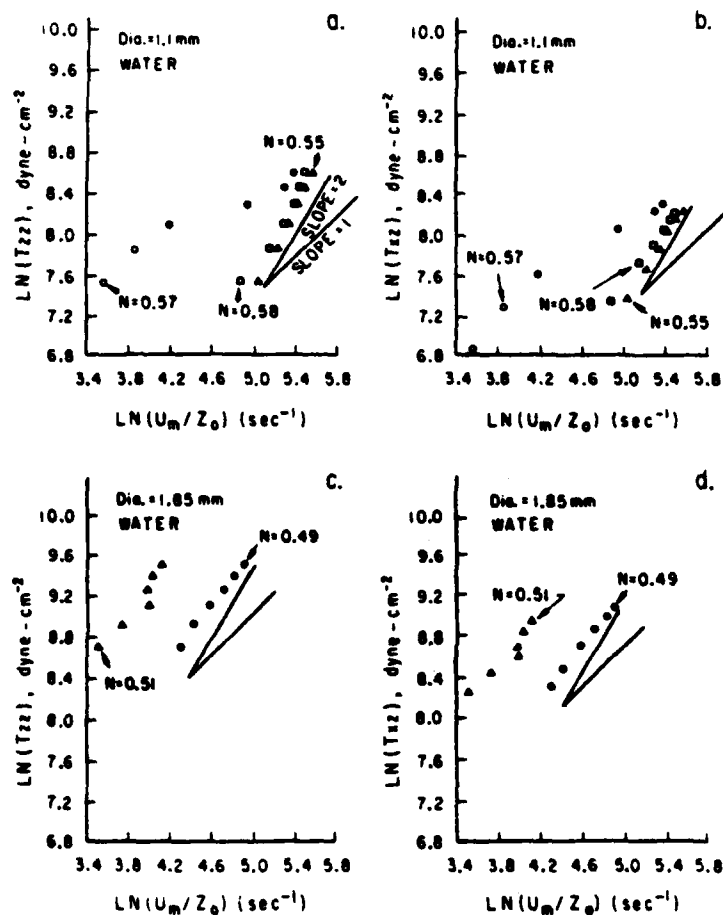
Figure 4-5. Ln stress vs ln shear rate for glass spheres in water (same data as Figure 4-2). Circles indicate data in the Bagnold's transition region (B<450). Slopes (at constant N) lie between one and two, indicating the dependence of the stresses upon the shear rate is between linear and quadratic.

models discussed, it appears that the water partially dampens the grain trajectories, and hence the velocity fluctuations of the grains, thus decreasing the impact during collisions.

The 18 experiments on fully shearing flows of 1.85 mm glass spheres in air are quite similiar to the experiments reported by Savage and Sayed (1983). The only significant difference between the experimental arrangements is that Savage and Sayed roughened the shearing surfaces with sandpaper, rather than cementing the actual grains being studied onto the surfaces as in the present experiments. Because both sets of data indicate the quadratic relationship between shear rate and stress which was originally observed by Bagnold, it would appear that the different surface characteristics both resulted in collisional type flows. However, it should be noted that the actual stress levels were greater in the present experiments than they were in Savage and Sayed's experiments (at equivalent concentrations and shear rates). For example, the shear stress developed by shearing 1.85 mm glass spheres at a concentration of 0.49 were about 3 times higher in the present experiments than those reported by Savage and Sayed for 1.8 mm glass spheres at the same concentration and shear rates. This difference is believed to result from the difference in materials at the upper and lower boundaries of the flow.

The dependence of the stresses upon the volume concentration is shown in Figures 4-6 to 4-8 as plotted points, together with the prediction curves of Bagnold, and Jenkins and Savage (superimposed), for all of the experiments in which air is the interstitial fluid. For Bagnold's relationship, N_m is the measured maximum volume concentration. For the 1.1mm spheres, $N_m=0.64$; for the 1.85 mm spheres, $N_m=0.55$;for the sand, $N_m=0.61$. The proportionality constants in Bagnold's model and α (assumed constant) in Jenkins and Savage's model are empirically fit, using a minimum squared error criterion. The coefficient of restitution, e, used in Jenkins and Savage's prediction is 0.9.

As seen in Figures 4-6 to 4-8, the stresses are only weakly dependent on the concentration up to approximately $N=0.5$ for the 1.1 mm spheres, and $N=0.45$ for the 1.85 cm spheres. Above these concentrations the stresses increase rapidly. The Bagnold curves describe this behavior quite well. The Jenkins and Savage curves predict the proper trend, but the curvature at $N=0.4$ to $N=0.5$ is not sharp enough. It is important to realize that Bagnold used his experimental results to determine the dependence of the stresses upon N, where Jenkins and Savage derive the dependence on N in the context of their 'kinetic' theory.

4.2 The stress ratio
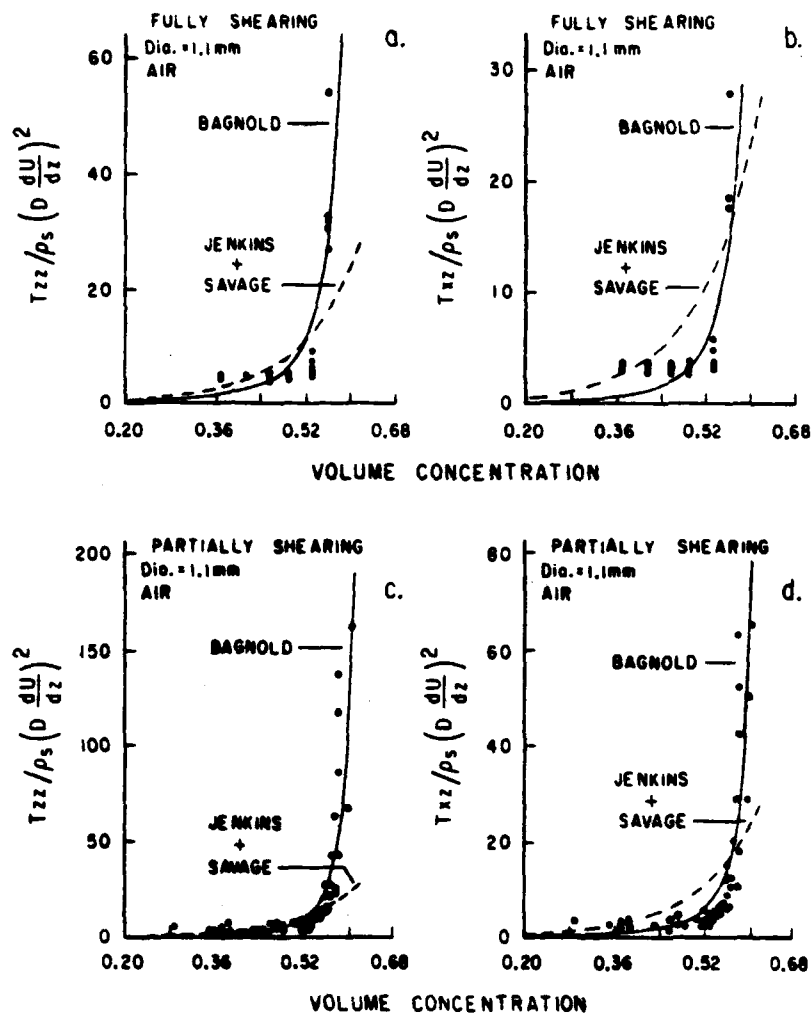
Figure 4-6. Nondimensional stress vs volume concentration for experiments on 1.1 mm glass spheres in air. The stresses are nondimensionalized by $\rho_s(DU')^2$ in order to isolate the influence of the volume concentration. Curves represent the predictions of Bagnold and of Jenkins and Savage.
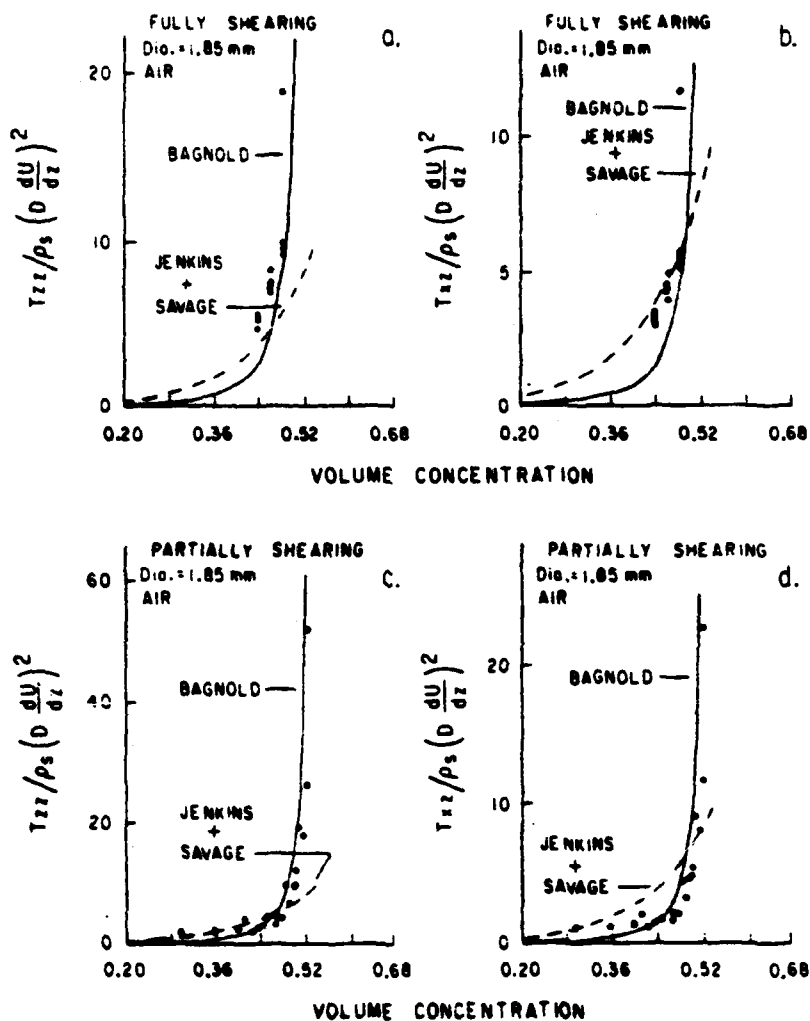
Figure 4-7. Nondimensional stress vs volume concentration for experiments on 1.85 mm glass spheres in air. The stresses are nondimensionalized by $\rho_s(DU')^2$ in order to isolate the influence of the volume concentration. Curves represent the predictions of Bagnold and of Jenkins and Savage.

PARTIALLY SHEARING
Dia.=0.55mm
AIR
BAGNOLD
JENKINS
+
SAVAGE
$T_{zz}/\rho_s\left(D\frac{dU}{dz}\right)^2$
VOLUME CONCENTRATION

PARTIALLY SHEARING b.
Dia.=0.55mm
AIR
BAGNOLD
JENKINS
+
SAVAGE
$T_{xz}/\rho_s\left(D\frac{dU}{dz}\right)^2$
VOLUME CONCENTRATION
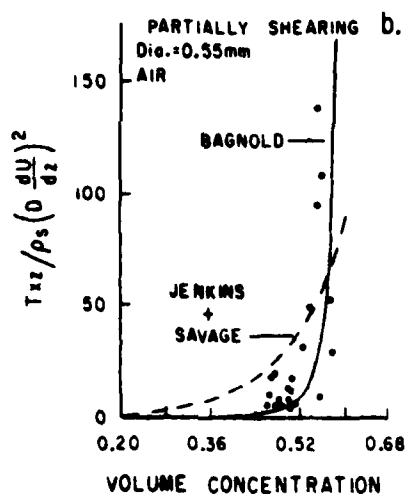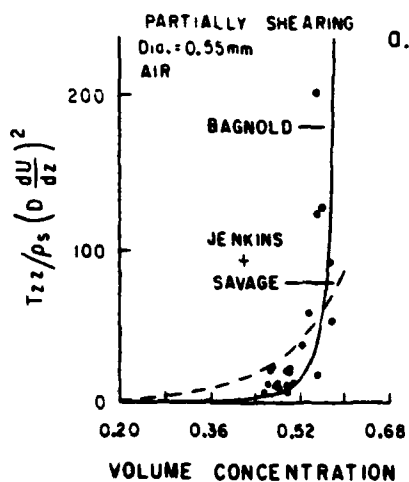
Figure 4-8. Nondimensional stress vs volume concentration for experiments on .55 mm sand in air. The stresses are nondimensionalized by $\rho_s(DU')^2$ in order to isolate the influence of the volume concentration. Curves represent the predictions of Bagnold and of Jenkins and Savage.

The stress ratio, T_{xz}/T_{zz} , evaluated at the lower boundary of the flow, reveals several consistent trends. The mean stress ratios, and their standard deviations, are given in Table 4-1. The standard deviations are approximately 10 percent of the mean, supporting the concept of a nearly constant stress ratio (over a range of shear rates and applied normal stresses) for a given material. Still, the variation from the means is not random. It correlates well with the shear rate, as will be shown.

Perhaps the most noticeable result is that the stress ratios for the fully shearing experiments are significantly higher than those resulting from the partially shearing flows. In terms of the momentum arguments presented in section 2, this observation indicates that if there were erodable grains at the lower boundary of the fully shearing flow, they would be mobilized into the shear flow. The solid lower boundary, although fully stressed from above, cannot partake in the granular fluctuations which would result in a higher normal stress. Thus there is a deficiency in the normal stress, and the stress ratios for the fully shearing flows are higher than the ratios for partially shearing flows.

This observation explains why Savage and Sayed's (1983) measurements of the stress ratio were higher than the dynamic angle of repose of the material. Because all of their experiments involved fully shearing conditions, the values of the stress ratio were higher than expected for a
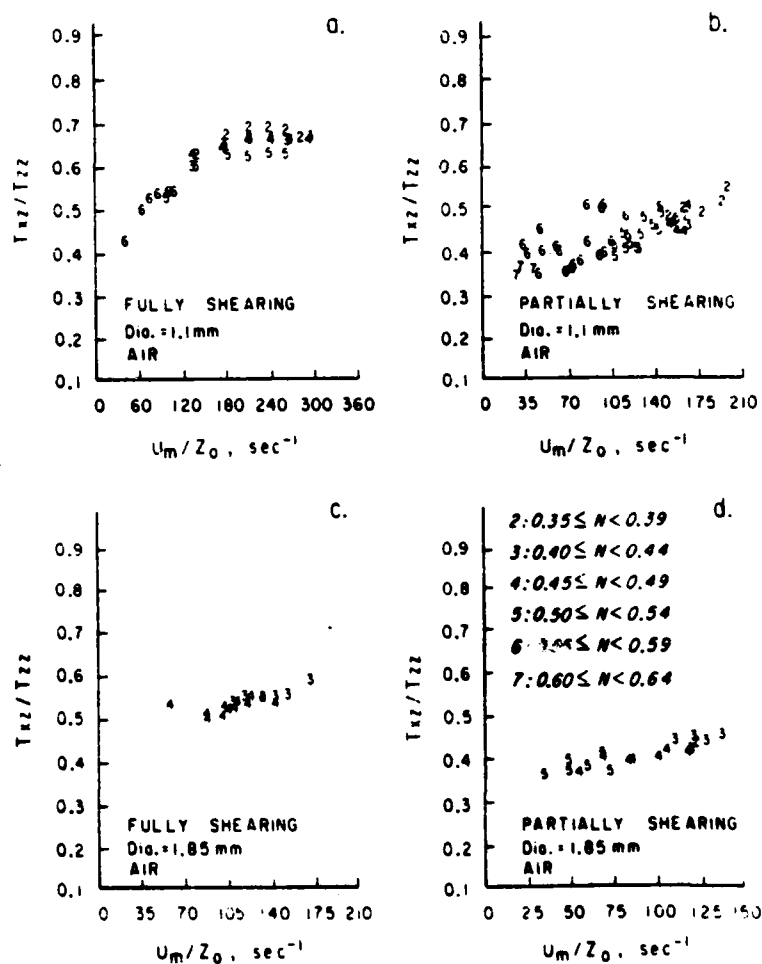
Figure 4-9. Stress ratio vs shear rate for glass spheres in air. Note sleight tendency for increasing ratios with increasing shear rate.
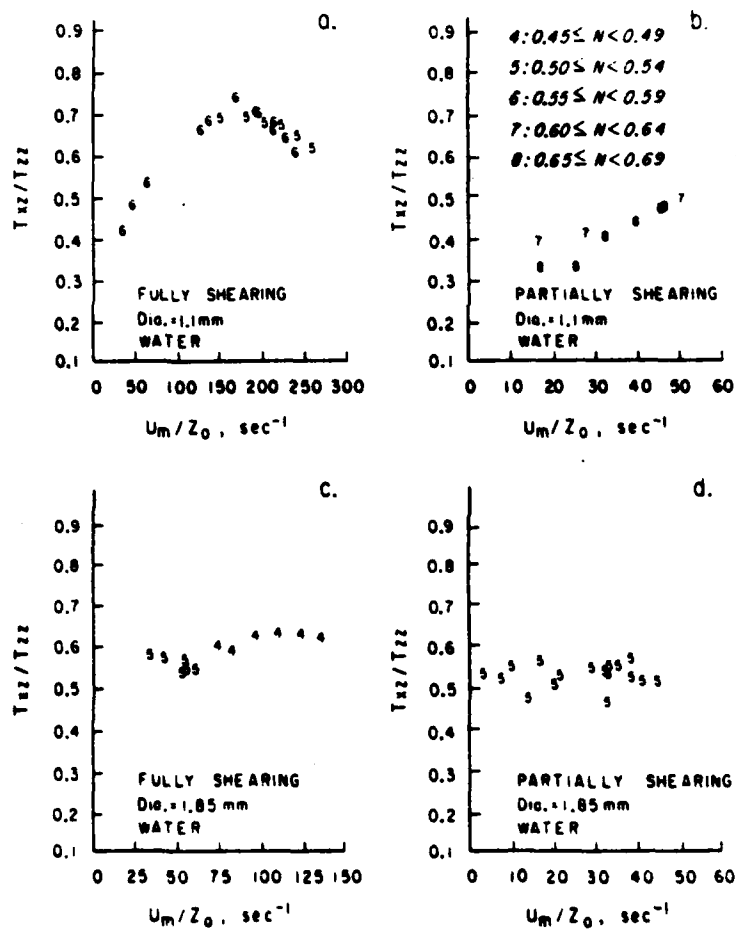
Figure 4-18. Stress ratio vs shear rate for glass spheres in water. Note sleight tendency for increasing ratios with increasing shear rate.
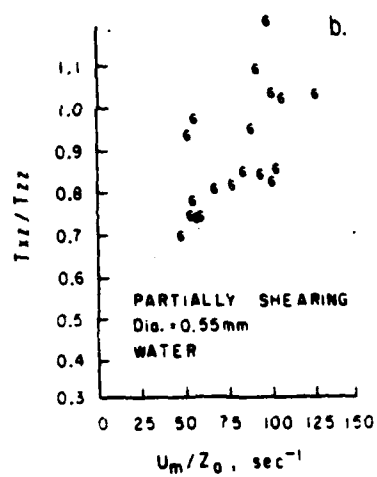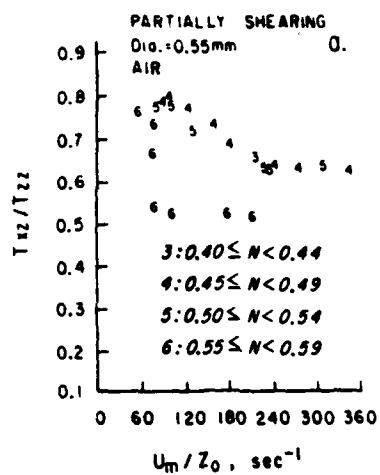
Figure 4-11. Stress ratio vs shear rate for sand.

Stress Ratio (mean (standard deviation))

	In air	In water
1.1 mm spheres		
fully shearing	0.63 (9.9%)	0.64 (13.1%)
partially shearing	0.44 (12.5%)	0.44 (17.8%)
1.85 mm spheres		
fully shearing	0.53 (3.9%)	0.59 (5.9%)
partially shearing	0.41 (8.5%)	0.53 (5.3%)
0.55 mm sand		
partially shearing	0.68 (13.7%)	0.89 (15.8%)

Table 4-1. The measured stress ratios

stress state close to the yield point. The measured stress
ratios, expressed as the inverse tangent of the stress
ratio, are compared to the dynamic angle of repose for the
various materials used in the present experiments in Table
4-2. The angle of repose consistently lies between the
friction angle for the partially shearing flow and the
friction angle for the fully shearing flow.

A second trend noticeable in the measurements of the
stress ratio is that the ratios for experiments in which
water is the interstitial fluid are sometimes higher (and
never lower) than those measured for experiments in which
air was the interstitial fluid.

There are at least two explanations for this
observation. The simplest explanation is that the
deformation of the interstitial water itself generates a
much higher shear stress than that generated by the
deformation of air. This stress adds to the shear stress
generated by granular interactions, resulting in a higher
stress ratio. However, because the fluid generated stresses
are much smaller than the granular stresses, this
explanation is not completely adequate.

A second explanation is is offered in the context of
the kinetic theories discussed in section 2. It follows
from equations 2-30 and 2-26 that the normal stress varies
directly with the pseudo-temperature, while the shear stress
depends upon the product of the shear rate and the square
root of the pseudo-temperature. One of the effects water

	$\tan^{-1}$(mean stress ratio) (degrees)		Dynamic angle of repose (degrees)
	in air	in water	
1.1 mm spheres			
fully shearing	32	33	26
partially shearing	24	24	
1.85 mm spheres			
fully shearing	28	31	28
partially shearing	22	28	
0.55 mm sand			
partially shearing	34	42	36

Table 4-2.   The measured friction angles and the dynamic
            angle of repose for the various materials.

has on the flow is that it decreases the pseudo-temperature by damping out vibrational motions, while maintaining the same mean velocities. Thus the stress ratio, which varies as the inverse of the square root of the pseudo-temperature, is higher when water is the interstitial fluid. Probably both the additional shear stress and the damping of granular vibrations due to the interstitial fluid viscosity contribute to the higher stress ratios measured when water was the interstitial fluid.

The dependence of the stress ratio upon the shear rate and volume concentration is shown in Figures 4-9 to 4-11. The ratio tends to increase with increasing shear rate, or decreasing volume concentration, particularly for the partially shearing experiments. This result will be used in the prediction of the immersed weight of the moving grains, in the next section.

4.3 Immersed weight of the shearing grains

In section 2 it was shown that the boundary between the nonshearing grains and the shearing grains in the partially shearing experiments can be explained by the conservation of momentum combined with a dynamic Coulomb yield criterion. The immersed weight of the moving grains was found to be described by:

$$\int_0^{Z_0} (\rho_s - \rho_f)\, Ng\, dz = \frac{\tau_0}{\tan(\phi_r)} - \tau_n \qquad 4\text{-}1$$

We will refer to the quantity on the left as the bedload,

because of its similarity to the concept of bedload in sediment transport theory.

Unforunately, the bedload is generally a small difference between the relatively large stresses, making its direct calculation somewhat unstable to slight errors in the stress measurements. Nevertheless, the data indicates there is clearly a predictive capability in estimating the bedload.

In applying equation 4-1 to predict the bedload, the results of the previous section are used to empirically express $\tan(\phi_r)$ as a linear function of shear rate:

$$\tan(\phi_r) = \tan(\phi_{r_0}) + \sqrt{6/g}\, K\, U' \qquad 4-2$$

The constants $\tan(\phi_{r_0})$ and K can be determined by means of a regression analysis of the measurements of the stress ratio described in the previous section. These constants are given in Table 4-3, along with the regression coefficients.

The measured bedload is compared to equation 4-1 in Figure 4-12. The correlation between equation 4-1 and the measured bedload is 0.664. For comparison, r=0.218 is significant at the .995 level for two random variables with an equivalent number of degrees of freedom. The symbol 'F' in Figure 4-12 represents data obtained under the highest applied normal stress. It is believed that the grains were abrading under these high stresses. The solid circles and numbers represent data obtained with sand, and have large errors associated with them.

	r	r(99%)	$\tan\phi_{r_o}$	K
In air				
1.1 mm spheres				
fully shearing	0.86	0.38	0.49	0.068
partially shearing	0.75	0.32	0.34	0.081
1.85 mm spheres				
fully shearing	0.78	0.52	0.46	0.045
partially shearing	0.87	0.49	0.32	0.069
0.55 mm sand				
partially shearing	-0.42	0.47	0.75	-0.060
In water				
1.1 mm spheres				
fully shearing	0.66	0.52	0.50	0.076
partially shearing	0.94	0.66	0.26	0.442
1.85 mm spheres				
fully shearing	0.80	0.61	0.53	0.060
partially shearing	0.02	0.53	0.53	0.004
0.55 mm sand				
partially shearing	0.61	0.50	0.60	0.490

Table 4-3. Results of regression analysis between the measured stress ratios and the shear rates. Terms are defined as:

$$\tan\phi_r = \tan\phi_{r_o} + \sqrt{D/g}\ K\ \frac{dU}{dz}$$
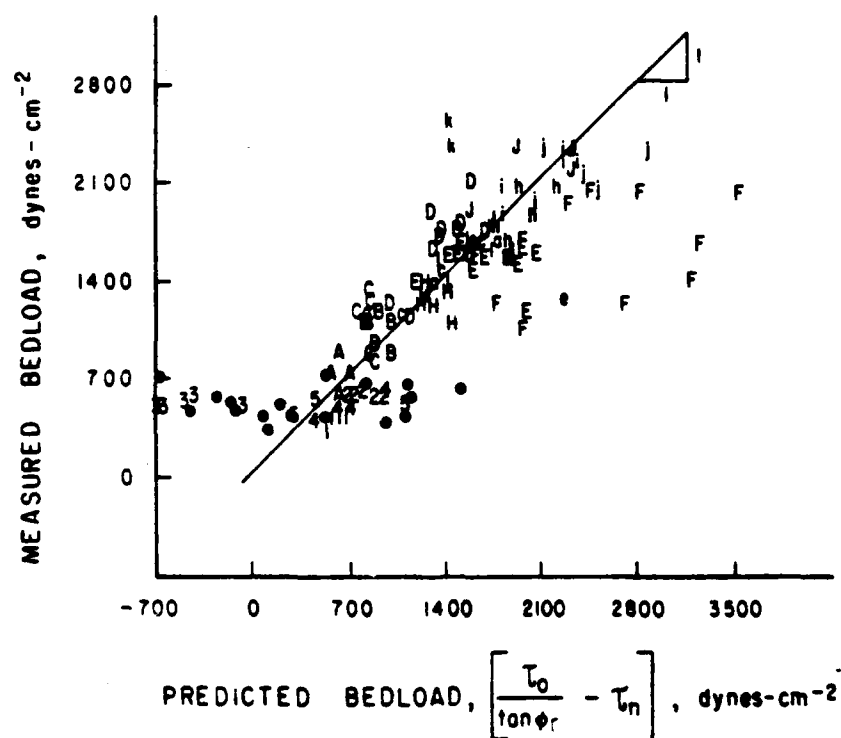
Figure 4-12. Measured bedload vs predicted bedload.
Prediction (equations 4-1 and 4-2) is based upon the
measurements of the stress ratio, and the application of a
dynamic Coulomb yield criterion.

The mean (for each material) predicted bedload is graphed against the mean measured bedload in Figure 4-13. The agreement is very good, as it should be, because the values of $\tan(\overline{\phi}_r)$ used in equation 4-1 are determined by averaging the actual measured values.

The correlations between the shear rate, the volume concentration and the bedload for the partially shearing experiments involving glass spheres are given in Table 4-4. For the dry experiments, the shear rate and the bedload are negatively correlated. This is consistent with the earlier observation of the positive correlation between the shear rate and $\tan\phi_r$. However, for the wet experiments, a positive correlation was observed between the shear rate and the bedload, even though the shear rate and $\tan\phi_r$ were still positively correlated (Table 4-3). This apparent paradox is explained by considering the relative importance of the shear stress transmitted by the interstitial fluid. As explained earlier, a more viscous interstitial fluid tends to decrease the pseudo-temperature. Hence both the normal stress, and the component of the shear stress which is generated by granular collisions are lower. The decrease in granular shear stress, however, is partially counterbalanced by an increase in interstitial fluid shear stress. So, as the shear rate increases, more grains can be moved by the increasing interstitial fluid shear stress, and the stress ratio can increase.
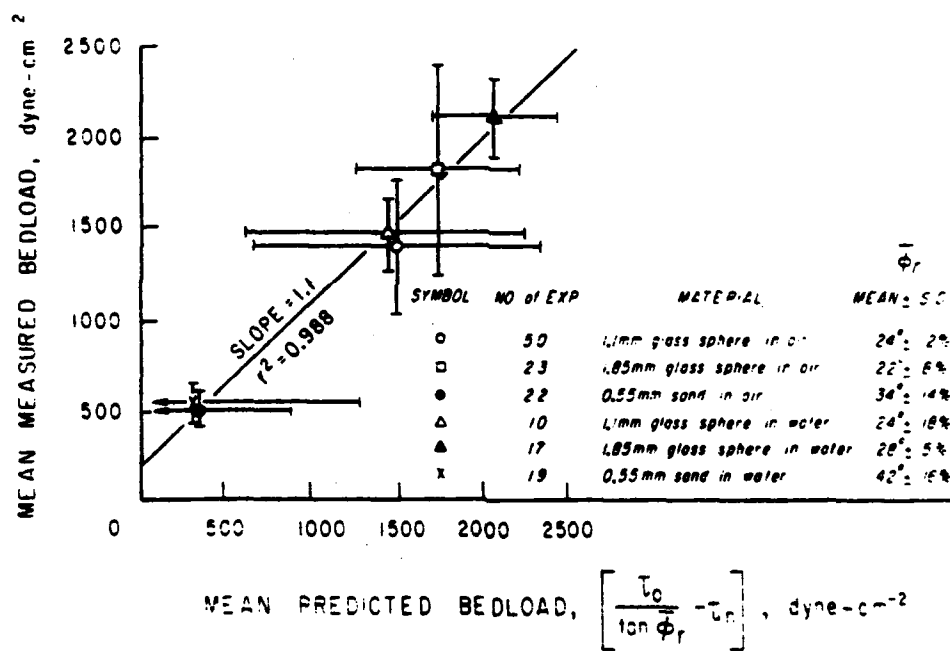
Figure 4-13. Mean measured bedload vs mean predicted bedload (for same data as Figure 4-12).

	Dia = 1.1 mm		Dia=1.85 mm	
	U'	N	U'	N
Bedload	-0.31	0.46	-0.57	0.65
IN				
U'	/	-0.86	/	-0.83
AIR				
	r(99%) = 0.32		r(99%) = 0.49	

	Dia = 1.1 mm		Dia=1.85 mm	
Bedload	0.80	-0.64	0.55	-0.25
IN				
U'	/	-0.56	/	-0.85
WATER				
	r(99%) = 0.66		r(99%) = 0.53	

Table 4-4. Correlations between the measured bedload,
shear rate, and volume concentration. The
99% significant correlations are also given.

4.4 The effects of grain angularity

The primary difference between glass spheres and coarse grained sands, in the context of these experiments, is the angularity of the grains. As seen in Figures 4-6 to 4-8 (note different scales), at constant N, the sand develops higher stresses than the spheres, particularly higher shear stresses. The stress ratio (Table 4-1) is significantly higher for sand, as is the angle of repose (Table 4-2).

An interesting effect of angularity was observed while prestressing the material by slowly shearing the material back and forth in an oscillatory manner.

As expected, when glass spheres were sheared in one direction, brought to a stop, and shearing started again in either the same or the opposite direction, the results were completely symmetric with respect to the direction and the sequence. The fact that shearing took place has no observable effect upon subsequent shearing as long as the motion comes to a complete stop between cycles.

For sand,however, some interesting effects of the deformation history on the static yield stress were observed. Furthermore, the effect was different for air or water as the interstitial fluid. In air, the static yield stress required to shear sand in the direction opposite to that in which it was just sheared was the same as the initial yield stress. The static yield stress required to

begin shearing in the same direction as the previous
shearing was higher than the intitial yield stress!
Presumably, as shearing ceases, the sand grains align into
an imbricated fabric which resists relative motion in the
direction of shearing, as shown schematically in Figure 4-
14.   Resumed shearing in the same direction is inhibited by
the anisotropically aligned grains; in contrast, motion in
the opposite direction need overcome only the usual sliding
friction.

When the sand was immersed in water, a different
behavior was observed. Resumed shearing in the same
direction required the same, or slightly less, stress than
the initial yield. Resumed shearing in the opposite
direction, in constrast, required a lesser stress to yield,
but then the yield was accompanied by a compaction of the
material (rather than the usual dilation), and a stress
equal to the initial yield stress was required to continue
shearing. This can be explained if the grains are left in
a loosely packed, but imbricated, state as shearing stops,
as shown schematically in Figure 4-15. Resumed shearing in
the same direction causes granular contact to steadily
increase, so the static yield stress will be required to
continue shearing. Resumed shearing in the opposite
direction initially has little resistance, until the grains
collapse back into a more densely packed state. The yield
stress will again then increase to its standard initial
value.

DIRECTION OF
ACCELERATION

DIRECTION OF
MOTION

ALIGNMENT
AFTER
SHEARING STOPS
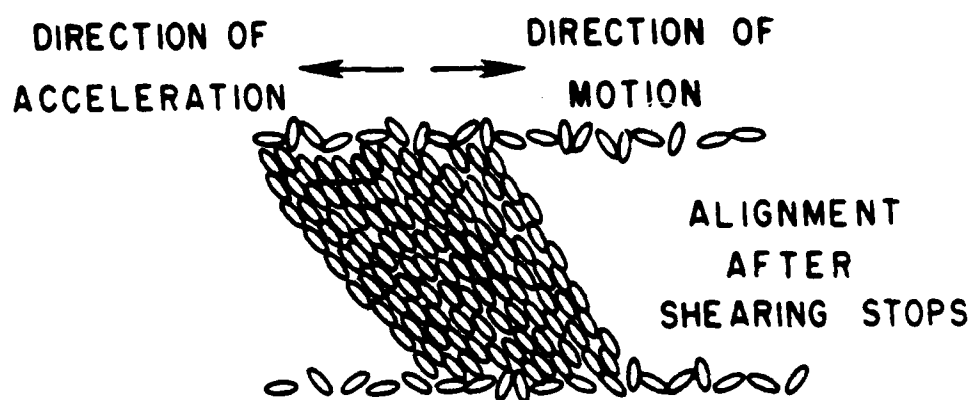
Figure 4-14.   Illustration of hypothesized
imbrication developed for sand being sheared in air.
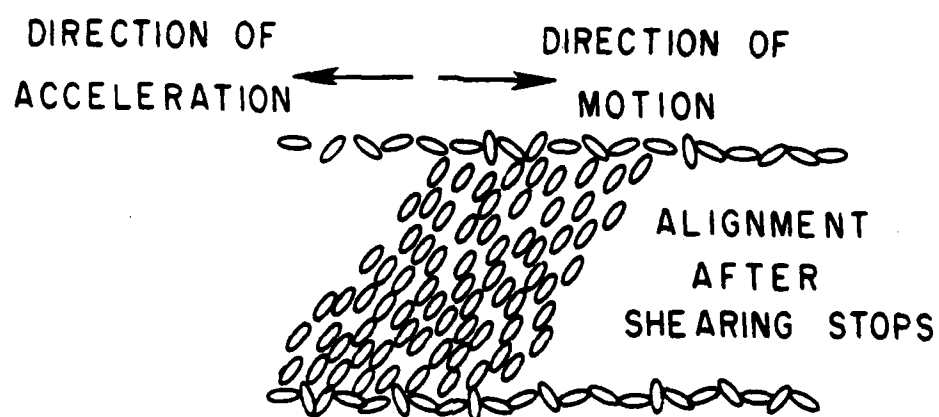
Figure 4-15.   Illustration of hypothesized
imbrication developed for sand being sheared in water.

5. Conclusions

This work addresses the subset of flows of granular materials known as rapidly flowing, granular-fluid materials. Experiments were conducted in an annular, parallel plate shear cell with two primary goals in mind. The first was to investigate the existence of an internal boundary above which the material deformed rapidly, but below which the material remained rigidly locked in place. The second goal was to examine the constitutive behavior of rapidly flowing granular-fluid materials bounded by parallel, roughened plates. The constitutive theories of McTigue(1979) and Jenkins and Savage(1983) are applied to study the steady, rapid flow of a semi-infinite granular bed under the influence of gravity and traction applied to its surface. Analytic solutions based upon McTigue's theory and numerical solutions based upon Jenkins and Savage's theory both suggest that there is a finite thickness of motion in the bed. For the limiting case where gravity is negligible and the material is fully shearing between parallel plates, the experiments can be directly compared to the analytic solutions given by Jenkins and Savage.

The experiments clearly demonstrate the existence of an internal boundary resulting in a finite thickness of the shearing layer. The thickness was measured to be between 5 and 15 grain diameters. This phenomenon occurs as a simple

result of momentum conservation in a gravity field. The
stresses at the boundary between the shearing and the
nonshearing regions conform to a dynamic Coulomb yield
criterion. For each of the granular-fluid materials, the
stress ratios at the boundary, T_{xz}/T_{zz} , were measured to be
nearly constant, with only a slight dependence upon the
shear rate and volume concentration.

The finite thickness of the shearing layer
illustrates an important problem in the mechanics of
granular materials which should be addressed: the rapid flow
regime needs to be systematically related to the less
intense quasi-static, or plastic regime of deformation in a
continuous and physically meaningful way. This is a
difficult task because of the very different mechanisms for
momentum transfer and energy dissipation in the two regimes.
Nontheless, most geophysical flows, and many industrial
flows involve a transition between the two regimes.
Matching the limits of these regimes is therefore of
paramount importance to understanding these granular flows.

The present experiments on the constitutive behavior
of rapidly flowing granular-fluid materials demonstrate that
when the interstitial fluid has no effect upon the
deformation, the stresses are quadratically dependent upon
the mean shear rate (at constant volume concentration).
These measurements confirm many of the observations of
Savage and Sayed(1983), which in turn support Bagnold's
hypothesis that granular collisions comprise the primary

mechanism by which momentum is tranferred in these flows.

The stresses were found (in the present study) to be weakly dependent on the volume concentration up to values of about 0.45 or 0.5. Above these concentrations, the stresses were strongly dependent on the volume concentration; sometimes the stresses increased by an order of magnitude with less than a 10% increase in the volume concentration. These observations are in agreement with those of Bagnold (1954). The kinetic theory of Jenkins and Savage (1983) correctly predicts an increase in the stress levels with increasing volume concentration, but the predicted increase is smaller than observed for volume concentrations greater than about 0.45.

The kinetic approach to rapidly flowing granular-fluid materials is rational and physically plausible. The theory of Jenkins and Savage(1983), although simplistic in its assumptions regarding granular interactions, predicts the dependence of the stresses upon the shear rate properly, and also predicts the trend of the dependence on the volume concentration. The kinetic approach will undoubtedly be improved by including such phenomenon as particle spin and friction. Further work is also needed in determining the exact nature of the collision anisotropy present in rapid shear flows. The effects of multiple collisions at high volume concentrations would also make a substantial improvement in the theory. As these improvements are implemented, the predicted dependence of the stresses upon

the volume concentration should improve.

The measured stress ratios, T_{xz}/T_{zz}, are higher for fully shearing flows than they are for partially shearing flows. This is a consequence of the rigid lower boundary of the fully shearing flows. Had there been erodable grains at this boundary, they would be mobilized into the flow, resulting in a greater mass of material in motion, and a lower stress ratio at the bottom of the flow.

Measurements of the stress ratios and of the constitutive behavior indicate that the interstitial fluid probably has a significant influence in many flows of interest. This is evidenced by the relatively higher stress ratios and the more linear dependence of the stresses on the shear rate for experiments in which water was the interstitial fluid. Probably both the shear stress supported by the deformation of the interstitial water, and the damping of grain trajectories by the water have a significant influence upon the mechanics of the granular-fluid, as suggested by Bagnold. A more rigorous theoretical basis for flows of this nature, where both granular collisions and interstitial fluid effects are important, needs to be developed. The limiting cases of a suspension of grains on the one hand, and the rapid collisional flow on the other, are fairly well formulated, and provide the asymptotic limits for future theories.

The experiments reported here provide new insights which aid in understanding some fundamental aspects of the

bedload sediment transport phenomenon.

Measurements of a nearly constant stress ratio at the level of no motion indicates there must always be a region of bedload transport if the fluid stress exceeds the threshold for motion. This follows from the fact that the fluid pressure is isotropic, so any normal stress at the level of no motion must be generated and transmitted by grain-to-grain interactions. Furthermore, as previously demonstrated, if the tangential component of the fluid stress on the bed is known, then the immersed weight of the grains participating in the bedload transport is predictable.

The present experiments suggest that a momentum based bedload transport model is close to being developed. Both the stresses at the lower boundary of the granular-fluid flow, and the constitutive behavior of the rapidly flowing region have been confirmed in this work. Once the rapidly flowing granular-fluid regime is tied smoothly into the dense suspension regime, the equations of motion will be well posed, and at least numerically solvable.

REFERENCES

Ackerman, N.L. and H. Shen, 1982, "Stresses in rapidly
    sheared fluid-solid mixtures," ASCE Journal of the
    Engineering Mechanics Division, v 108, no 1, p 95-113.

Bagnold, R.A., 1941, "The physics of blown sand and desert
    dunes," William Morrow and Co., New York, 265 pp.

Bagnold, R.A., 1954, "Experiments on a gravity-free
    dispersion of large solid spheres in a Newtonian fluid
    under shear," Royal Society (London) Proc., ser. A,v 225,
    p 49-63.

Bagnold, R.A., 1956, "The flow of cohesionless grains in
    fluids," Philos. Trans. of the Royal Soc. of London, ser.
    A, v 249, no. 964, p 235-297.

Bagnold, R.A., 1966, "An approach to the sediment transport
    problem from general physics," U.S. Geological Survey
    Professional Paper, 422-J, 37 pp.

Bailard, J.A., 1978, "An Experimental Study of Granular-
    Fluid Flow," Ph.D. dissertation, Univ of Calif. at San
    Diego, pp. 172.

Bailard, J.A., and D.L. Inman, 1979, "A re-examination of
    Bagnold's granular fluid model and bed load transport
    equation," Journal of Geophysical Research,
    v.84,no.C12,p7827-33.

Cambell, C.S., 1982,"Shear flows of granular materials,"
    Ph.D. dissertation, California Institute of Technology,
    pp. 259.

Carr, J.F., and D.M. Walker, 1968, "An annular shear cell for
    granular materials," Powder Technology, v 1, N 370, p.
    369-373.

Cheng, C.D. and R.A. Richmond,1978,"Some observations on the
    rheological behaviour of dense suspensions," Rheological
    Acta, v. 17,p.446-453.

Coulomb, C.A., 1773, "Essai sur une application des regles de
    maximis st minimus a quelque problemes de statique
    relatifs a l'architecture," Acad. R. Sci. Mem. Math.
    Phys. par divers savants, v 7, p. 343-382.

de Josselin de Jong, G., 1959, "Statics and kinematics in the
    failable zone of a granular material,", Ph.D.
    dissertation, Delft University.

de Josselin de Jong, G., 1971, "The double sliding free rotating model for granular assemblies," Geotechnique, v 21, p. 155-163.

Drucker, D.C. and W. Prager, 1952, "Soil mechanics and plastic analysis of limit design," Quarterly of Applied Mathematics, v 10, p157-165.

Goodman, M.A. and S.C. Cowin, 1972, "A continuum theory for granular material," Archives for Rational Mechanics and Analysis, v. 44, p. 249-266.

Inman, D.L., 1953, "Areal and seasonal variations in beach and nearshore sediments at La Jolla, California," Beach Erosion Board, Corps of Engineers Tech. Memo 39, 134 pp.

Inman, D.L., G.C. Ewing, and J.B. Corliss, 1966, "Coastal sand dunes of Guerrero Negro, Baja California, Mexico," Geol. Soc. Amer. Bull., v. 77, no 8, p787-802.

Inman, D.L., and D.M. Hanes, 1980, "Field measurements of bed and suspended load motion in the surf zone," in Proc. of the 17th Int. Conf. on Coastal Engineering, abstracts vol., 456 pp.

Inman, D.L., 1983, Teaching notes:SIO 216 , Physics of Sediment Transport, University of California,San Diego.

Ishida M, and T. Shirai, 1979, "Velocity distributions in the flow of solid particles in an inclined open channel," Journal of Chemical Engineering of Japan, v 12, p 46-50.

Jenike, A.W., and R.T. Shield, 1959, "On the plastic flow of Coulomb solids beyond original failure," Journal of Applied Mechanics, v 26, p.599-602.

Jenkins, J.T., and S.C. Cowin, 1979, "Theories for flowing granular materials," Mechanics applied to the transport of bulk materials, A.S.M.E.,AMD-31,p.79-89.

Jenkins, J.T., and S.B. Savage, 1983, "A theory for the rapid flow of identical, smooth, nearly elastic spherical particles," Journal of Fluid Mechanics,   .

Komar, P.D., and D.L. Inman, 1970, "Longshore sand transport on beaches," Journal of Geophysical Research, v.76, no.15, p.5914-5927.

Lowe, D.R., 1976, "Grain flow and grain flow deposits," Journal of Sedimentary Petrology, v 46, no 1, p 188-199.

Mandl G. and R.F. Luque, 1970, "Fully developed plastic shear flow of granular materials," Geotechnique, v 20, no 3, p277-307.

McTigue, D.F., 1979, "A nonlinear continuum model for flowing granular materials," Ph.D. dissertation, Stanford University.

McTigue, D.F., 1982, "A nonlinear constitutive model for granular materials: application to gravity flow," Journal of Applied Mechanics, v 49, p 291-296.

Mehrabadi, M.M. and S.C. Cowin, 1978, "Initial planar deformation of dilatant granular materials," Journal of the Mechanics and Physics of Solids, v 26, p. 269-284.

Ogawa, S., 1978, "Multitemperature theory of granular materials," Proceedings of the U.S.-Japan Seminar on Continuum-Mechanical and Statistical Approaches in the Mechanics of Granular Materials,(Cowin, S.C. and Satake, M., eds.) Gakujutsu Bunken Fukyukai, Tokyo, Japan, p. 208-217.

Ogawa, S., A. Umemura, and N. Oshima, 1980, "On the equations of fully fluidized granular materials," J. Appl. Math. Phys. (ZAMP), v 31, p 483-493.

Owen, P.R.,1964, "Saltation of uniform grains in air," Journal of Fluid Mechanics, v.20, part 2, p.225-242.

Passman, S.L., Nunziato, J.W., Bailey, P.B., and J.P. Thomas,Jr., 1980, " Shearing flows of granular materials," The Journal of the Engineering Mechanics Division, Proc. ASCE, v 106, no EM4, p. 773-783.

Reynolds, O., 1885, "On the dilatancy of media composed of rigid particles is contact," Phil. Mag., 5th series, v 20, p. 469-481.

Savage, S.B., 1978, "Experiments on shear flows of cohesionless granular materials," Proceedings of the U.S.-Japan Seminar on Continuum-Mechanical and Statistical Approaches in the Mechanics of Granular Materials (Cowin, S.C. and Satake, M. eds.),Gakujutsu Bunken Fukyu-kai, p. 241-254.

Savage, S.B., 1979, "Gravity flow of cohesionless granular materials in chutes and channels," Journal of Fluid Mechanics, v 92, p. 53-96.

Savage S.B., and D.J. Jeffrey, 1981, "The stress tensor in a granular flow at high shear rates," Journal of Fluid Mechanics, v 110, p 255-272.

Savage, S. B., and M. Sayed, 1983, "Stresses developed by dry cohesionless granular materials sheared in an annular shear cell", Journal of Fluid Mechanics,(in press).

Savage, S. B., and S. McKeown, 1983, "Shear stresses
    developed during rapid shear of concentrated suspensions
    of large spherical particles between concentric
    cylinders," Journal of Fluid Mechanics, v 127, p 453-472.

Sayed, M., 1980,"Theoretical and experimental studies on dry
    cohesionless granular materials," Ph.D. dissertation,
    McGill University, pp 157.

Spencer, A.J.M., 1964, "A theory of the kinematics of ideal
    soils under plain strain conditions," J. of the Mechanics
    and Physics of Solids, v 12, p 337-351.

Terzaghi, K., 1943, Theoretical Soil Mechanics, Wiley, .

Vermeer, P.A. and H.J. Luger (eds.), 1982, Deformation and
    Failure of Granular Materials, Balkema, pp 661.

Yalen, M.S., 1972, "Mechanics of sediment transport,"
    Pergamon Press, New York, pp. 290.

APPENDIX: DATA

Fully shearing 1.1 mm glass spheres in air

Exp	N	Um/Zo (1/sec.)	Shear stress	Applied normal stress	Normal stress (dyne/cm/cm)	Stress ratio at z=Zo	Zo (mm.)
1	0.56	41.	1443.	2191.	3360.	0.43	8.6
2	0.56	66.	2418.	3627.	4796.	0.50	8.6
3	0.56	77.	3295.	5063.	6232.	0.53	8.6
4	0.56	88.	4143.	6499.	7668.	0.54	8.6
5	0.56	103.	4933.	7935.	9104.	0.54	8.6
6	0.56	111.	5733.	9371.	10540.	0.54	8.6
7	0.54	101.	1784.	2191.	3360.	0.53	9.0
8	0.54	140.	2896.	3627.	4796.	0.60	9.0
9	0.54	185.	3929.	5063.	6232.	0.63	9.0
10	0.54	214.	4806.	6499.	7668.	0.63	9.0
11	0.54	242.	5762.	7935.	9104.	0.63	9.0
12	0.54	267.	6659.	9371.	10540.	0.63	9.0
13	0.49	136.	2106.	2191.	3360.	0.63	9.8
14	0.49	180.	3149.	3627.	4796.	0.66	9.8
15	0.49	214.	4134.	5063.	6232.	0.66	9.8
16	0.49	246.	5099.	6499.	7668.	0.67	9.8
17	0.49	272.	6054.	7935.	9104.	0.67	9.8
18	0.49	298.	7000.	9371.	10540.	0.66	9.8
19	0.46	136.	2023.	2191.	3360.	0.60	10.5
20	0.46	178.	3134.	3627.	4796.	0.65	10.5
21	0.46	216.	4178.	5063.	6232.	0.67	10.5
22	0.46	245.	5123.	6499.	7668.	0.67	10.5
23	0.46	274.	6079.	7935.	9104.	0.67	10.5
24	0.46	300.	7093.	9371.	10540.	0.67	10.5
25	0.42	136.	2033.	2191.	3360.	0.61	11.5
26	0.42	179.	3164.	3627.	4796.	0.66	11.5
27	0.42	215.	4187.	5063.	6232.	0.67	11.5
28	0.42	245.	5162.	6499.	7668.	0.67	11.5
29	0.42	272.	6118.	7935.	9104.	0.67	11.5
30	0.42	299.	7112.	9371.	10540.	0.68	11.5
31	0.37	140.	2111.	2191.	3360.	0.63	13.0
32	0.37	180.	3222.	3627.	4796.	0.67	13.0
33	0.37	214.	4304.	5063.	6232.	0.69	13.0
34	0.37	243.	5279.	6499.	7668.	0.69	13.0
35	0.37	267.	6225.	7935.	9104.	0.68	13.0
36	0.37	288.	7003.	9371.	10540.	0.67	13.0

Partially shearing 1.1 mm glass spheres in air.

Exp	N	Um/Zo (1/sec.)	Shear stress	Applied normal stress	Normal stress at z=Zo (dyne/cm/cm)	Stress ratio	Zo (mm.)
37	0.58	48.	3503.	6499.	7748.	0.45	7.3
38	0.56	87.	4009.	6499.	7926.	0.51	8.7
39	0.56	100.	4141.	6499.	8194.	0.50	10.4
40	0.56	99.	4249.	6499.	8551.	0.50	12.5
41	0.56	118.	4107.	6499.	8551.	0.48	12.5
42	0.55	132.	4063.	6499.	8551.	0.48	12.8
43	0.52	147.	4102.	6499.	8461.	0.49	12.8
44	0.47	169.	4097.	6499.	8194.	0.50	12.3
45	0.37	200.	4230.	6499.	7748.	0.55	11.5
46	0.29	196.	4303.	6499.	7570.	0.57	12.7
47	0.58	34.	2600.	5063.	6242.	0.42	6.9
48	0.58	37.	2595.	5063.	6591.	0.39	9.0
49	0.58	50.	2648.	5063.	6634.	0.40	9.3
50	0.57	62.	2755.	5063.	6722.	0.41	9.9
51	0.57	87.	2755.	5063.	6547.	0.42	9.0
52	0.56	107.	2794.	5063.	6634.	0.42	9.7
53	0.55	116.	2930.	5063.	6678.	0.44	10.1
54	0.53	144.	2891.	5063.	6460.	0.45	9.0
55	0.53	146.	3312.	5063.	6656.	0.50	10.3
56	0.51	158.	3111.	5063.	6656.	0.47	10.8
57	0.46	153.	3096.	5063.	6745.	0.46	12.5
58	0.39	153.	3175.	5063.	6628.	0.48	13.9
59	0.60	33.	1954.	3627.	5385.	0.36	10.0
60	0.61	28.	1793.	3627.	5250.	0.34	9.2
61	0.60	43.	1934.	3627.	5430.	0.36	10.3
62	0.58	73.	1978.	3627.	5520.	0.36	11.2
63	0.58	75.	2104.	3627.	5746.	0.37	12.6
64	0.54	109.	2216.	3627.	5385.	0.41	11.2
65	0.53	122.	2211.	3627.	5340.	0.41	11.1
66	0.56	101.	2128.	3627.	5385.	0.39	10.7
67	0.51	140.	2390.	3627.	5220.	0.46	10.8
68	0.43	168.	2233.	3627.	4866.	0.46	9.9
69	0.35	167.	2296.	3627.	4778.	0.48	11.3
70	0.57	64.	1497.	2909.	3750.	0.40	6.1
71	0.58	69.	1492.	2909.	4262.	0.35	9.7
72	0.54	109.	1585.	2909.	4116.	0.38	9.2
73	0.52	128.	1688.	2909.	4168.	0.40	9.9
74	0.47	160.	1786.	2909.	4020.	0.44	9.7
75	0.37	180.	1855.	2909.	3798.	0.49	9.9
76	0.39	165.	1536.	2191.	3080.	0.50	9.4
77	0.49	157.	1457.	2191.	3154.	0.46	8.2
78	0.52	130.	1438.	2191.	3302.	0.44	8.9
79	0.54	118.	1330.	2191.	3302.	0.40	8.6
80	0.55	97.	1310.	2191.	3376.	0.39	8.9
81	0.57	81.	1241.	2191.	3302.	0.38	8.1
82	0.58	46.	1138.	2191.	3302.	0.34	7.8

83	0.53	120.	962.	1473.	2214.	0.43	5.7
84	0.52	128.	942.	1473.	2362.	0.40	7.1
85	0.46	165.	976.	1473.	2214.	0.44	6.7
86	0.36	196.	1060.	1473.	2066.	0.51	6.7

Fully shearing 1.85 mm glass spheres in air.

Exp	N	Um/Zo (1/sec.)	Shear stress	Applied normal stress	Normal stress at z=Zo (dyne/cm/cm)	Stress ratio	Zo (mm.)
87	0.49	59.	3802.	5063.	7215.	0.53	16.2
88	0.49	90.	4290.	6499.	8651.	0.50	16.2
89	0.49	102.	5070.	7935.	10087.	0.50	16.2
90	0.49	107.	5947.	9371.	11523.	0.52	16.2
91	0.49	112.	6824.	10807.	12959.	0.53	16.2
92	0.49	122.	7604.	12243.	14395.	0.53	16.2
93	0.46	89.	3656.	5063.	7215.	0.51	17.0
94	0.46	104.	4533.	6499.	8651.	0.52	17.0
95	0.46	114.	5411.	7935.	10087.	0.54	17.0
96	0.46	125.	6288.	9371.	11523.	0.55	17.0
97	0.46	134.	7068.	10807.	12959.	0.55	17.0
98	0.46	144.	7653.	12243.	14395.	0.53	17.0
99	0.44	110.	3851.	5063.	7215.	0.53	18.0
100	0.44	120.	4728.	6499.	8651.	0.55	18.0
101	0.44	133.	5508.	7935.	10087.	0.55	18.0
102	0.44	144.	6288.	9371.	11523.	0.55	18.0
103	0.44	154.	7166.	10807.	12959.	0.55	18.0
104	0.44	172.	8433.	12243.	14395.	0.59	18.0

Partially shearing 1.85 mm glass spheres in air.

Exp	N	Um/Zo (1/sec.)	Shear stress	Applied normal stress	Normal stress at z=Zo (dyne/cm/cm)	Stress ratio	Zo (mm.)
105	0.53	35.	2624.	5063.	7267.	0.36	15.4
106	0.52	50.	2727.	5063.	7414.	0.37	16.4
107	0.52	61.	2796.	5063.	7414.	0.38	16.7
108	0.50	73.	2732.	5063.	7414.	0.37	17.1
109	0.45	118.	2879.	5063.	6973.	0.41	15.5
110	0.41	128.	3021.	5063.	6900.	0.44	16.3
111	0.51	49.	2061.	3627.	5243.	0.39	11.6
112	0.50	70.	2086.	3627.	5243.	0.40	11.9
113	0.50	69.	2140.	3627.	5243.	0.41	11.8
114	0.49	85.	2086.	3627.	5317.	0.39	12.6
115	0.47	106.	2169.	3627.	5207.	0.42	12.3
116	0.45	119.	2164.	3627.	5170.	0.42	12.6
117	0.40	137.	2282.	3627.	5023.	0.45	12.8
118	0.49	56.	1283.	2191.	3535.	0.36	10.1
119	0.48	86.	1386.	2191.	3514.	0.39	10.1
120	0.47	101.	1435.	2191.	3587.	0.40	10.9
121	0.43	122.	1528.	2191.	3403.	0.45	10.4
122	0.36	123.	1498.	2191.	3440.	0.44	12.7
123	0.44	111.	1537.	2191.	3514.	0.44	11.1
124	0.30	130.	1621.	2191.	3293.	0.49	13.6

Partially shearing 0.55 mm sand in air.

Exp	N	Um/Zo (1/sec.)	Shear stress	Applied normal stress	Normal stress at z=Zo	Stress ratio	Zo (mm.)
					(dyne/cm/cm)		
125	0.47	90.	1332.	1333.	1673.	0.80	2.8
126	0.47	98.	1418.	1333.	1749.	0.81	3.4
127	0.47	125.	1373.	1333.	1753.	0.78	3.5
128	0.46	160.	1302.	1333.	1753.	0.74	3.5
129	0.43	217.	1166.	1333.	1753.	0.67	3.8
130	0.56	55.	2609.	2769.	3373.	0.77	4.2
131	0.54	81.	2624.	2769.	3341.	0.79	4.1
132	0.53	101.	2629.	2769.	3341.	0.79	4.2
133	0.51	130.	2422.	2769.	3341.	0.73	4.4
134	0.50	182.	2326.	2769.	3341.	0.70	4.4
135	0.58	78.	2563.	4205.	4701.	0.55	3.3
136	0.58	102.	2488.	4205.	4701.	0.53	3.3
137	0.56	177.	2508.	4205.	4739.	0.53	3.7
138	0.51	213.	2493.	4205.	4778.	0.52	4.4
139	0.56	77.	4567.	5641.	6136.	0.74	3.5
140	0.48	246.	3916.	5641.	6049.	0.65	3.3
141	0.48	280.	3926.	5641.	6123.	0.64	3.9
142	0.50	313.	4047.	5641.	6271.	0.64	4.9
143	0.55	74.	6091.	8513.	9004.	0.68	3.4
144	0.50	236.	5702.	8513.	8962.	0.64	3.5
145	0.50	232.	5818.	8513.	9074.	0.64	4.4
146	0.49	350.	5727.	8513.	9037.	0.63	4.2

Fully shearing 1.85 mm glass spheres in water.

Exp	N	Um/Zo (1/sec.)	Shear stress	Applied normal stress	Normal stress at z=Zo (dyne/cm/cm)	Stress ratio	Zo (mm.)
175	0.51	34.	3802.	5063.	6527.	0.58	16.6
176	0.51	42.	4582.	6499.	7963.	0.57	16.6
177	0.51	54.	5362.	7935.	9399.	0.57	16.6
178	0.51	54.	5850.	9371.	10835.	0.54	16.6
179	0.51	56.	6727.	10807.	12271.	0.55	16.6
180	0.51	62.	7507.	12243.	13707.	0.55	16.6
181	0.50	75.	3948.	5063.	6527.	0.61	16.9
182	0.50	84.	4728.	6499.	7963.	0.59	16.9
183	0.50	98.	5898.	7935.	9399.	0.63	16.9
184	0.50	111.	6873.	9371.	10835.	0.63	16.9
185	0.50	125.	7751.	10807.	12271.	0.63	16.9
186	0.50	136.	8531.	12243.	13707.	0.62	16.9

Partially shearing 1.85 mm glass spheres in water.

Exp	N	Um/Zo (1/sec.)	Shear stress	Applied normal stress	Normal stress at z=Zo (dyne/cm/cm)	Stress ratio	Zo (mm.)
187	0.53	9.	3753.	5063.	7037.	0.53	21.2
188	0.53	22.	3997.	5063.	7131.	0.56	22.5
189	0.52	35.	3948.	5063.	7225.	0.55	23.8
190	0.52	44.	4192.	5063.	7413.	0.57	25.9
191	0.51	50.	3802.	5063.	7413.	0.51	26.2
192	0.53	13.	2876.	3627.	5507.	0.52	20.4
193	0.52	26.	2876.	3627.	5695.	0.50	22.8
194	0.52	38.	3169.	3627.	5883.	0.54	25.1
195	0.51	39.	3120.	3627.	5883.	0.53	25.1
196	0.51	44.	3120.	3627.	5977.	0.52	26.2
197	0.53	16.	2145.	2191.	3883.	0.55	18.3
198	0.52	27.	2096.	2191.	3977.	0.53	19.8
199	0.51	39.	2242.	2191.	4071.	0.55	21.1
200	0.51	41.	2340.	2191.	4259.	0.55	23.3
201	0.50	46.	2194.	2191.	4259.	0.51	23.6
202	0.52	19.	4192.	6499.	8849.	0.47	25.7
203	0.52	38.	4192.	6499.	9037.	0.46	28.1

Partially shearing 0.55 mm sand in water.

Exp	N	Um/Zo (1/sec.)	Shear stress	Applied normal stress	Normal stress at z=Zo (dyne/cm/cm)	Stress ratio	Zo (mm.)
204	0.57	53.	2947.	2769.	3153.	0.94	4.2
205	0.58	57.	3113.	2769.	3201.	0.97	4.7
206	0.58	90.	3043.	2769.	3201.	0.95	4.7
207	0.57	92.	3658.	2769.	3345.	1.09	6.3
208	0.57	99.	4097.	2769.	3393.	1.21	6.9
209	0.59	68.	3653.	4205.	4541.	0.81	3.6
210	0.58	78.	3785.	4205.	4637.	0.82	4.6
211	0.59	85.	4007.	4205.	4733.	0.85	5.6
212	0.58	104.	4037.	4205.	4733.	0.85	5.7
213	0.58	107.	4975.	4205.	4877.	1.02	7.2
214	0.58	55.	4728.	5641.	6073.	0.78	4.7
215	0.57	61.	4557.	5641.	6160.	0.74	5.7
216	0.58	95.	5187.	5641.	6169.	0.84	5.7
217	0.57	101.	6530.	5641.	6301.	1.04	7.3
218	0.56	127.	6550.	5641.	6349.	1.03	7.9
219	0.57	49.	6247.	8513.	8985.	0.69	5.2
220	0.57	54.	6666.	8513.	8985.	0.74	5.2
221	0.57	58.	6676.	8513.	9079.	0.74	6.2
222	0.57	102.	7599.	8513.	9221.	0.82	7.7

Fully shearing 1.1 mm glass spheres in water.

Exp	N	Um/Zo (1/sec.)	Shear stress	Applied normal stress	Normal stress	Stress ratio at z=Zo	Zo (mm.)
					(dyne/cm/cm)		
147	0.57	35.	941.	1473.	2252.	0.42	9.5
148	0.57	47.	1428.	2191.	2970.	0.48	9.5
149	0.57	66.	1964.	2909.	3688.	0.53	9.5
150	0.57	140.	3027.	3627.	4406.	0.69	9.5
151	0.57	200.	3612.	4345.	5124.	0.70	9.5
152	0.57	216.	3866.	5063.	5842.	0.66	9.5
153	0.58	131.	1497.	1473.	2252.	0.66	9.3
154	0.58	172.	2189.	2191.	2970.	0.74	9.3
155	0.58	198.	2608.	2909.	3688.	0.71	9.3
156	0.58	218.	2998.	3627.	4406.	0.68	9.3
157	0.58	231.	3290.	4345.	5124.	0.64	9.3
158	0.58	243.	3554.	5063.	5842.	0.61	9.3
159	0.55	155.	1560.	1473.	2252.	0.69	9.9
160	0.55	186.	2057.	2191.	2970.	0.69	9.9
161	0.55	208.	2506.	2909.	3688.	0.68	9.9
162	0.55	227.	2964.	3627.	4406.	0.67	9.9
163	0.55	245.	3315.	4345.	5124.	0.65	9.9
164	0.55	264.	3607.	5063.	5842.	0.62	9.9

Partially shearing 1.1 mm glass spheres in water.

Exp	N	Um/Zo (1/sec.)	Shear stress	Applied normal stress	Normal stress	Stress ratio at z=Zo	Zo (mm.)
165	0.66	26.	882.	1473.	2657.	0.33	12.4
166	0.65	40.	1258.	1473.	2855.	0.44	14.7
167	0.64	51.	1521.	1473.	3052.	0.50	16.9
168	0.64	64.	1843.	1473.	3151.	0.58	18.1
169	0.67	17.	1365.	2909.	4093.	0.33	12.3
170	0.65	33.	1784.	2909.	4389.	0.41	15.6
171	0.65	47.	2208.	2909.	4587.	0.48	17.8
172	0.65	17.	2506.	5063.	6357.	0.39	13.8
173	0.64	28.	2744.	5063.	6645.	0.41	17.1
174	0.66	46.	3193.	5063.	6741.	0.47	17.7

END

DATE
FILMED

1-84